

AD A 182931

REPORT SD-TR-87-34

TR-0086(6935-05)-2

Effects on Advanced Materials:
Results of the STS-8 EOIM Experiment

M. J. MESHISHNEK, W. K. STUCKEY,
J. S. EVANGELIDES, L. A. FELDMAN, and R. V. PETERSON
Materials Sciences Laboratory
Laboratory Operations

and

G. S. ARNOLD and D. R. PEPLINSKI
Chemistry and Physics Laboratory
The Aerospace Corporation
El Segundo, CA 90245

20 July 1987

Prepared for

SPACE DIVISION
AIR FORCE SYSTEMS COMMAND
Los Angeles Air Force Station
P.O. Box 92960, Worldway Postal Center
Los Angeles, CA 90009-2960

APPROVED FOR PUBLIC RELEASE:
DISTRIBUTION UNLIMITED

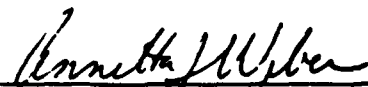
87 7 27 045

This report was submitted by The Aerospace Corporation, El Segundo, CA 90245, under Contract No. F04701-85-C-0086 with the Space Division, P.O. Box 92960, Worldway Postal Center, Los Angeles, CA 90009-2960. It was reviewed and approved for The Aerospace Corporation by R. W. Fillers, Director, Materials Sciences Laboratory, and S. Feuerstein, Director, Chemistry and Physics Laboratory.

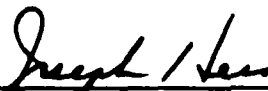
Capt Annetta Weber/CNIV was the project officer for the Mission-Oriented Investigation and Experimentation (MOIE) Program.

This report has been reviewed by the Public Affairs Office (PAS) and is releasable to the National Technical Information Service (NTIS). At NTIS, it will be available to the general public, including foreign nationals.

This technical report has been reviewed and is approved for publication. Publication of this report does not constitute Air Force approval of the report's findings or conclusions. It is published only for the exchange and stimulation of ideas.



ANNETTA WEBER, Capt, USAF
MOIE Project Officer
SD/CNIV



JOSEPH HESS, GM-15
Director, AFSTC West Coast Office
AFSTC/WCO OL-AB

90245,
92960,
and app
Material
Physic

Orient

relea
will

Publi
repor
stim

AM
MO
SD

THE AEROSPACE CORPORATION

DOCUMENT CHANGE NOTICE

to: Copyholder, Report SD-TR-87-34 cc: 1674
Aerospace Report No.
TR-0086(6935-05)-2

DATE: 29 July

SUBJECT: Correction of Aerospace Report Number

FROM: Reports
MAIL STATION: MI/111
BLDG: A4
EXT: 65630

Please make the following change to your copy of "Effects on Advanced Mate
Results of the STS-8 EOIM Experiment" (20 July 1987):

On the first page, DD Form 1473, change the Aerospace Report No. from
TR-0086(6925-05)-2 to TR-0086(6935-05)-2.

UNCLASSIFIED

SECURITY CLASSIFICATION OF THIS PAGE

REPORT DOCUMENTATION PAGE

1a. REPORT SECURITY CLASSIFICATION Unclassified		1b. RESTRICTIVE MARKINGS	
2a. SECURITY CLASSIFICATION AUTHORITY		3. DISTRIBUTION / AVAILABILITY OF REPORT Approved for public release; distribution unlimited.	
2b. DECLASSIFICATION / DOWNGRADING SCHEDULE			
4. PERFORMING ORGANIZATION REPORT NUMBER(S) TR-0086(69)5-05)-2		5. MONITORING ORGANIZATION REPORT NUMBER(S) SD-TR-87-34	
6a. NAME OF PERFORMING ORGANIZATION The Aerospace Corporation Laboratory Operations	6b. OFFICE SYMBOL (if applicable)	7a. NAME OF MONITORING ORGANIZATION Space Division	
6c. ADDRESS (City, State, and ZIP Code) El Segundo, CA 90245		7b. ADDRESS (City, State, and ZIP Code) Los Angeles, CA 90009-2960	
8a. NAME OF FUNDING / SPONSORING ORGANIZATION Space Division	8b. OFFICE SYMBOL (if applicable) AFSTC/WCO	9. PROCUREMENT INSTRUMENT IDENTIFICATION NUMBER F04701-85-C-0086	
8c. ADDRESS (City, State, and ZIP Code) Los Angeles, CA 90009-2960		10. SOURCE OF FUNDING NUMBERS	
		PROGRAM ELEMENT NO.	PROJECT NO.
		TASK NO.	WORK UNIT ACCESSION NO.
11. TITLE (Include Security Classification) EFFECTS ON ADVANCED MATERIALS: RESULTS OF THE STS-8 EOIM EXPERIMENT			
12. PERSONAL AUTHOR(S) M. J. Meshishnek, W. K. Stuckey, J. S. Evangelides, L. A. Feldman, G. S. Arnold, D. B. Peplinski, and R. V. Peterson			
13a. TYPE OF REPORT	13b. TIME COVERED FROM TO	14. DATE OF REPORT (Year, Month, Day) 1987 July 20	15. PAGE COUNT 91
16. SUPPLEMENTARY NOTATION Approved for public release; distribution unlimited.			
17. COSATI CODES			18. SUBJECT TERMS (Continue on reverse if necessary and identify by block number)
FIELD	GROUP	SUB-GROUP	
19. ABSTRACT (Continue on reverse if necessary and identify by block number)			
Atomic oxygen		Fourier transform infrared spectroscopy (FTIR)	
Auger analysis		Graphite	
Carbon fibers		High-temperature coatings	
Fiberglass		Infrared optical coatings	
A variety of materials were exposed to the low Earth orbit space environment on shuttle flight STS-8 as a part of NASA's "Effects of Oxygen Atoms Interaction with Materials" experiment. These materials included carbon fibers and graphites, infrared optical materials, organic and metal films, Kevlar and fiberglass fabric, and high-temperature coatings. The effects noted on these materials included oxidative erosion of the carbon and graphite, loss of tensile strength for the Kevlar fabric, erosion and oxidation of organic films, partial oxidation of infrared optical materials, and loss of reflectance for the high-temperature coatings.			
20. DISTRIBUTION / AVAILABILITY OF ABSTRACT. <input type="checkbox"/> UNCLASSIFIED/UNLIMITED <input checked="" type="checkbox"/> SAME AS RPT. <input type="checkbox"/> DTIC USERS		21. ABSTRACT SECURITY CLASSIFICATION Unclassified	
22a. NAME OF RESPONSIBLE INDIVIDUAL		22b. TELEPHONE (Include Area Code)	22c. OFFICE SYMBOL

DD FORM 1473, 84 MAR

83 APR edition may be used until exhausted.
All other editions are obsolete.

SECURITY CLASSIFICATION OF THIS PAGE

UNCLASSIFIED

PREFACE

The authors wish to thank the following individuals for their technical assistance in this work: Ann Bertrand, Eugene Borson, Richard Brose, Paul Chaffee, Sandra Gyetvay, David Hanna, Martin Leung, Nicholas Marquez, Thomas Park, Gloria To, Lucio Tolentino, and Clark Williams.

CONTENTS

PREFACE.....	1
I. INTRODUCTION.....	9
II. OPTICAL MATERIALS AND COATINGS.....	13
A. Infrared Optical Materials.....	13
B. Indium Oxide and Indium Tin Oxide.....	17
C. Polished Nickel Mirror.....	18
III. ORGANIC AND METAL FILMS.....	21
A. Experimental Procedure.....	21
B. Results.....	25
C. Conclusions.....	38
IV. STS-8 KEVLAR AND FIBERGLASS SAMPLES.....	43
A. Experimental Procedure.....	43
B. Results.....	43
C. Conclusions.....	47
V. CARBON FIBERS AND GRAPHITES.....	51
A. Sample Description.....	51
B. Experimental Procedure.....	51
C. Results and Discussion.....	51
D. Summary and Conclusions.....	63
VI. HIGH-TEMPERATURE COATINGS.....	71
A. Introduction.....	71
B. Sample Description.....	71
C. Experimental Procedure.....	72
D. Results.....	73
E. Conclusions.....	84
REFERENCES.....	91

FIGURES

1.	STS-8 Specimen Identification Format.....	12
2.	The Aerospace Organic and Metallic Thin-Films Tray.....	22
3.	Schematic of Tray Function.....	23
4.	FTIR Spectrum of Organic Thin Films: Preflight Apiezon (ATR Mode).....	26
5.	FTIR Spectrum of Organic Thin Films: Postflight Apiezon (ATR Mode).....	27
6.	FTIR Spectrum of Organic Thin Films: Preflight Silicone (ATR Mode).....	28
7.	FTIR Spectrum of Organic Thin Films: Postflight Silicone (ATR Mode).....	29
8.	FTIR Spectrum of Organic Thin Films: Kapton, Exposed Area (Transmission Mode).....	30
9.	FTIR Spectrum of Organic Thin Films: Kapton, Masked Area (Transmission Mode).....	31
10.	FTIR Spectrum of Organic Thin Films: Epoxy, Exposed Area (Transmission Mode).....	32
11.	FTIR Spectrum of Organic Thin Films: Epoxy, Masked Area (Transmission Mode).....	33
12.	FTIR Spectrum of Collector Plates: Silicone Collector Plate (ATR Mode).....	34
13.	FTIR Spectrum of Collector Plates: Kapton Collector Plate (ATR Mode).....	35
14.	FTIR Spectrum of Collector Plates: Apiezon Collector Plate (ATR Mode).....	36
15.	FTIR Spectrum of Collector Plates: Epoxy Collector Plate (ATR Mode).....	37
16.	Typical IMMA Profile for an "Up" Sample.....	40
17.	Photographs STS-8 Aerospace-Fabricated Holder for Kevlar and Fiberglass Samples (Preflight).....	44

FIGURES (Continued)

18.	Photograph of Kevlar from Flight Tray 2, Showing Surface Sheen Dulled by O-Atom Exposure.....	45
19.	Graphite Crystal Structure Showing Large Anisotropy.....	52
20.	Photomicrographs of Xenon-Ion Etching of Polished Surface to Enhance Viewing of Graphite Basal-Plane Orientation.....	54
21.	Scanning Electron Micrograph of Mounted Carbon Filaments in Cross Section.....	56
22.	Scanning Electron Micrographs of KGF 200.....	57
23.	Scanning Electron Micrographs of Low-Temperature PAN.....	58
24.	Scanning Electron Micrographs of Thornel 300.....	59
25.	Scanning Electron Micrographs of HM 3000.....	60
26.	Scanning Electron Micrograph of HM 3000, Showing Center Core Region.....	61
27.	Scanning Electron Micrograph of HM 3000 Filament after Oxidation in Air at Atmospheric Pressure and a Temperature of ~3900°C.....	62
28.	Scanning Electron Micrographs of VSB 32.....	64
29.	Scanning Electron Micrographs of Kevlar Polyamid.....	65
30.	Scanning Electron Micrographs of the A-Plane in Pyrolytic Graphite.....	66
31.	Scanning Electron Micrographs of the C-Plane in Pyrolytic Graphite.....	67
32.	Scanning Electron Micrographs (Cross-Sectional View) of Conical Features in Oxidized Pyrolytic Graphite.....	68
33.	Scanning Electron Micrographs of POCO 5Q Polycrystalline Graphite.....	69
34.	Scanning Electron Micrographs of POCO 5Q Polycrystalline Graphite, Showing Changes in Micropore Diameters.....	70

FIGURES (Continued)

35.	Auger Surface Profiles of Polished Mo, Showing Oxygen Depth Profile.....	79
36.	Photomicrographs of Mo/Cr/Black Cr Sample, Showing Cracking and Scaling Caused by Exposure.....	81
37.	Auger Surface Profiles of Black Cr on Cr on Mo, Showing Oxygen Depth Profile.....	82
38.	Photomicrograph of Mo/Cr/Black Cr Sample, Showing Debonding of Surface Layer and Exposed Cr Undercoating.....	83
39.	Auger Depth Profile of Black Ir Coating, Showing Oxygen Depth Profile.....	85
40.	Scanning Electron Micrographs and Oxygen Depth Profile of Black Ir on Mo Coating.....	86
41.	Photomicrograph of Black Rh on Mo Coating of STS-8 Flight Sample, Showing Pattern of Ring-Like Mottling.....	87
42.	Photomicrographs of KAT Glass on Mo Coating.....	88

TABLES

1.	STS-8 Aerospace Disk Specimens (Langley Research Center Holder Assembly, Tray 2).....	10
2.	STS-8 Aerospace EOIM Disk Specimens (Tray 1).....	11
3.	Infrared Optical Material Samples.....	14
4.	Postflight BRDF Summary.....	19
5.	Materials and Results of Organic Thin Films.....	24
6.	Thickness of Oxide Film on Silver.....	39
7.	STS-8 Kevlar Mechanical Testing Data.....	48
8.	Filament Property Data.....	53
9.	STS-8 High-Temperature Coating Experiment: Visual Observations.....	74
10.	STS-8 High-Temperature Coating Experiment: FTIR Difference Spectra (4000 to 500 cm^{-1}) for Samples Having Changes in Appearance.....	75
11.	STS-8 High-Temperature Coating Experiment: FTIR Difference Spectra (4000 to 500 cm^{-1}) for Samples Having No Change in Appearance.....	76
12.	STS-8 High-Temperature Coating Experiment: Adherence Test.....	78

I. INTRODUCTION

The Aerospace Corporation participated in the National Aeronautics and Space Administration (NASA) Effects of Oxygen Interaction with Materials (EOIM) experiments on shuttle missions STS-5 and STS-8. These experiments were designed to study the reactions of a wide variety of typical spacecraft materials with oxygen in low Earth orbit. The results obtained from the STS-8 experiment will be described, along with some comparisons to previously unpublished STS-5 results.

The samples on STS-8 were contained in one of the trays provided by NASA's Langley Research Center as well as in an Aerospace-designed tray. The samples in the Langley tray are listed in Table 1. Table 2 shows the locations of the samples in the Aerospace tray. Samples A, B, and C were 1 in. in diameter; the others were 0.5 in. in diameter. Sample locations for both trays are indicated in Figs. 1a and 1b. In addition, Aerospace designed and built two additional fixtures for specific experiments. These two fixtures contained the organic and metal film experiment and the Kevlar and fiberglass experiment. (These fixtures are described in Sections III and IV, respectively.) Thus, four separate trays were the responsibility of The Aerospace Corporation in the EOIM experiment on flight STS-8.

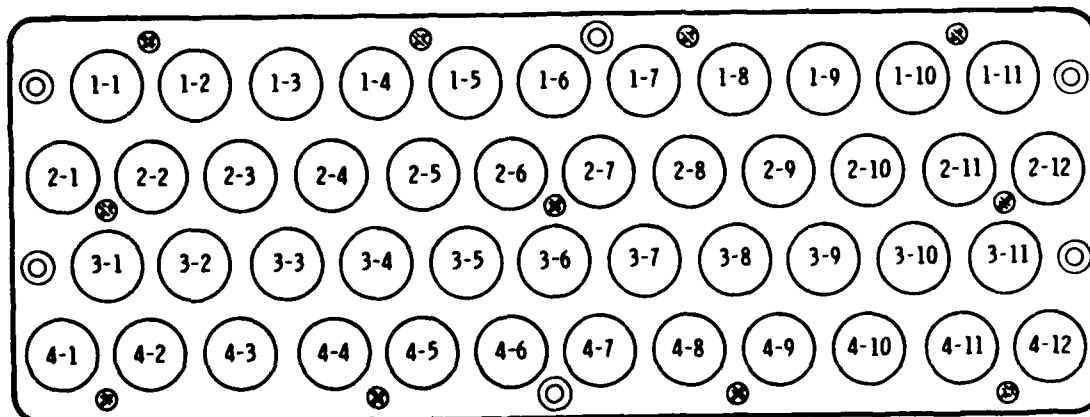
The following technical discussion applies to those samples analyzed at Aerospace. (Some of the samples in the trays were contributed by others -- Jet Propulsion Laboratory, Aerojet, Martin-Marietta -- and will be reported independently.) The samples are divided into the following categories: optical materials and coatings, organic and metal films, Kevlar and fiberglass, carbon fibers and graphites, and high-temperature coatings. For this experiment, the shuttle's payload bay was maintained into the velocity vector for about 40 h at an altitude of roughly 120 nmi; the result was a calculated atomic oxygen (O) fluence of 3.5×10^{20} atoms cm^{-2} (see Ref. 1).

Table 1. STS-8 Aerospace Disk Specimens (Langley Research Center Holder Assembly, Tray 2)

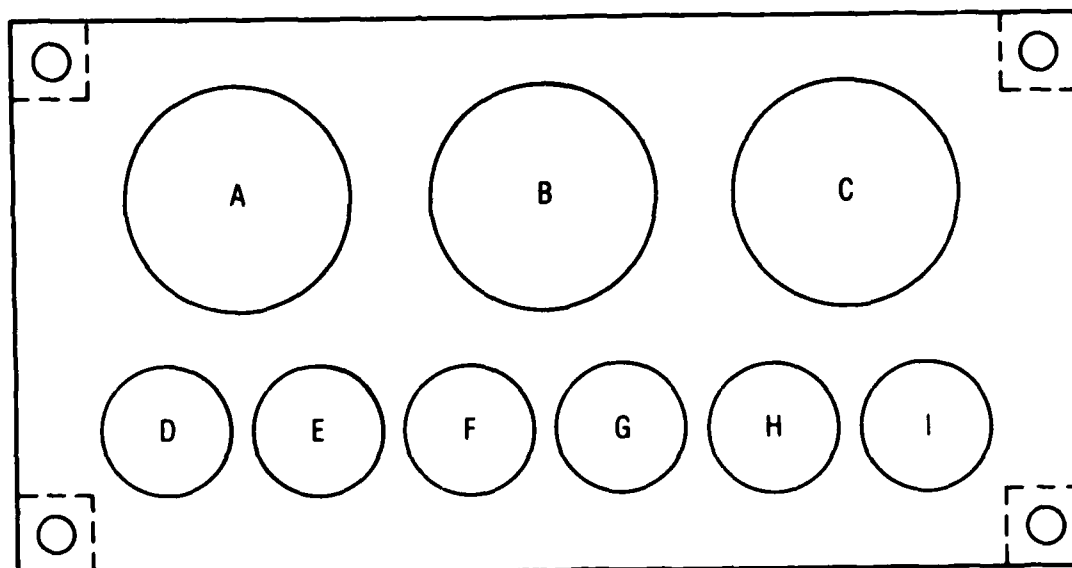
Specimen	Quantity	Location
graphite/Mg	1	1-1
bare graphite coating	1	1-2
pyrolytic graphite ("a" face)	1	1-3
Ir on Mo	1	1-4
Mo (polished)	1	1-5
Be	1	1-6
graphite/Mg/Ti	1	2-1
siloxane-treated graphite coating	1	2-2
black epoxy paint on Al	1	2-3
black Rh on Mo	1	2-4
sputtered black Rh	1	2-5
Ti ("tiodized")	1	2-6
Flamemaster S1023 on Al	1	3-1
IR optics	1	3-2
Ti 6-4 ("tiodized")	1	3-3
Ir foil	1	3-4
M-diethynyl-benzene + ethynyl-benzene (1:1)	1	3-5
Kevlar (up)/Ag (down)	1	4-1
IR optics	1	4-2
Z306 on Kapton	1	4-3
Rh foil	1	4-4
Mg foil AZ61A	<u>1</u>	4-5
Total	22	

Table 2. STS-8 Aerospace EOIM Disk Specimens (Tray 1)

Specimen	Quantity	Location
ITO/Kapton composite	1	A
SAS on Al	1	B
black Kapton	1	C
ZnO	1	D
Ag	1	E
pyrolytic graphite ("c" face)	1	F
fibers (HM 3000/Kevlar/low-temperature PAN/KGF 200/mesophase pitch/T300)	1	G
AXF-5Q-POCO Graphite	1	H
silicone	<u>1</u>	I
Total	9	



A



B

Fig. 1. STS-8 Specimen Identification Format. (a) Langley Research Center disk holders. (b) Aerospace tray.

II. OPTICAL MATERIALS AND COATINGS

A. INFRARED OPTICAL MATERIALS

1. SAMPLE DESCRIPTION

An increase in the background noise level of the Earth sensor assembly (ESA) of the DMSP spacecraft and their sister craft from the NOAA/TIROS program has been observed on orbit. This increase is consistent with a decrease of approximately 20% in the transmission of the objective lens of the ESA. The timing and geometry of the anomaly suggest that atomic oxygen in the atmosphere may play a role in that degradation.²

To investigate the role of atomic oxygen (O) in the DMSP ESA offset anomaly, samples of coated infrared optical materials were flown on both the STS-5 and STS-8 EOIM experiments. These samples are described in Table 3.

Samples on the STS-5 experiment were flown in duplicate, one in the "up" (exposed) position and one in the "down" (unexposed) position. Only one exposed sample each was flown on STS-8.

2. EXPERIMENTAL PROCEDURE

a. Chemical Composition

Postflight measurements of the surface chemical composition of the disks were made by x-ray photoelectron spectroscopy (XPS) using a McPherson ESCA-36 spectrometer. The chemical depth profiles of two of the STS-5 samples were measured with a Physical Electronics model 590 scanning Auger microprobe equipped with a 5-kV argon-ion sputtering beam.

b. Infrared (IR) Transmission

IR transmission spectra of the disks from 2 to 20 μm were measured with a Nicolet MX-1 Fourier transform infrared (FTIR) spectrophotometer having a beam diameter of 7 mm. Pre- and postflight measurements of the STS-8 samples were performed, and transmission spectra of the STS-5 samples were compared to those of replicate samples maintained in the laboratory.

Table 3. Infrared Optical Material Samples

Sample No.	Flight	Substrate	Coating
A51A	STS-5	germanium	MLAR,* with ZnS as its outermost coating
A51B	STS-5	germanium	MLAR, with ThF ₄ as its outermost coating
A51C	STS-5	silicon	MLAR, with SiO _x as its outermost coating
3-2	STS-8	germanium	same as 51B
4-2	STS-8	germanium	ZnS, 1/4-wave optical thickness at 15 μm

* Multilayer antireflection coating

3. RESULTS

a. Chemical Composition

XPS measurements revealed that all of the flight samples with ZnS coatings were partially oxidized, although the "up" sample from STS-5 was more heavily oxidized than the "down" sample. In each of these samples less sulfur (S) was present than in the laboratory control sample. Comparison of the intensity ratios of O and S to zinc (Zn) as zinc oxide (ZnO) and zinc sulfide (ZnS) showed that the stoichiometry of the samples changes as a function of O-atom exposure. The ZnS found in the exposed and unexposed samples was sulfur deficient compared to that in the laboratory sample; the ZnO was more oxygen rich. Chemical depth-profile measurements of the "up" ZnS sample showed a ZnS layer of approximately 2 μm , with an initial intermixed oxide layer of approximately 20 nm. Surface contaminants of carbon (C) and chlorine (Cl) were also observed.

The XPS results for the STS-8 ZnS samples differed from those for the STS-5 samples. ZnS was less completely oxidized, appearing as a ZnSO_4 layer ~4 A thick, or as a 0.4:1 mixture of ZnSO_4 and ZnS in the 30-A sampling depth of the instrument. This result is surprising, inasmuch as the fluence in the STS-8 exposure was approximately three times as great as that on the earlier flight.

XPS measurements of thorium fluoride (ThF_4)-coated samples from both flights showed that exposed samples were oxidized. A layer of thorium dioxide (ThO_2) 10 A thick, or a 1:1 mixture of ThO_2 and ThF_4 throughout the sampled depth of 30 A, was formed. In the STS-5 samples, the relative amount of F with respect to Th present as ThF_4 remained constant: ThO_2 replaced some of the ThF_4 , but the fluoride remained stoichiometric. This was unlike the case for ZnS, where the ZnS in the flown samples was sulfur deficient compared to that in the laboratory samples. The STS-8 sample exhibited higher oxygen content than did the STS-5 sample, which is qualitatively consistent with the higher fluence on the later flight. No oxidation was observed on the unexposed STS-5 sample. The chemical depth profile of the STS-5 ThF_4 "up" sample revealed a multilayer structure, including ThF_4 layers. Carbon and

oxygen were interspersed throughout the multilayer structure, suggesting that they may have been incorporated in the manufacturing process.

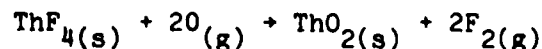
b. Infrared Transmission

No significant changes in the infrared transmission of any of the ThF₄- or ZnS-coated samples were observed. A slight decrease in transmission of the SiO_x-coated samples (compared to a laboratory control sample) was measured.

4. DISCUSSION

Oxidation of the ZnS on the flight samples is not a surprising result, inasmuch as the high-temperature oxidation of ZnS in air is a well-known process.³ However, since the infrared transmission spectra of ZnO and ZnS exhibit only subtle differences in the midwavelength IR, one would not expect the thin oxide layer formed to produce a significant change in the coating absorbance.

The result, that the STS-5 "up" and STS-8 ThF₄ samples were oxidized while the STS-5 "down" sample was not, is intuitively satisfying. Assuming that oxidation proceeds via the reaction



one might expect the process to be endothermic by as much as 2.9 eV. However, if one includes the additional translational energy of the incident atomic oxygen in the accounting, the process can be exothermic by more than 7 eV. Indeed, the lack of oxidation of the ThF₄ "down" sample (when other "down" samples of silver and ZnS were oxidized) lends some credence to the notion that the initial translational energy of the atomic oxygen is effective in promoting the oxidation of ThF₄. However, this is thin evidence on which to base a firm conclusion.

The surface analysis of the SiO_x samples provided no explanation of the apparent decrease in transmission of these materials. They were, however, located nearest to the 250°F tray on the STS-5 experiment. It is possible that some contamination was produced by the hot tray, although the infrared

spectra neither confirm nor deny this notion. Since transmission spectra of the STS-5 samples were compared to laboratory control samples rather than to preflight measurements, the possibility of systematic error must be admitted. Otherwise, the origin of this apparent transmission loss remains unclear.

B. INDIUM OXIDE AND INDIUM TIN OXIDE

Conductive, transparent coatings of indium tin oxide (ITO) are normally applied to spacecraft surfaces to inhibit charging. Three types of samples with ITO or indium oxide (In_2O_3) coatings were included: (1) silica disks with 200, 400, and 600-Å-thick coatings of ITO; (2) an In_2O_3 -coated second surface mirror, or optical solar reflector (OSR), from Optical Coating Laboratories, Inc.; and (3) six strips of ITO-coated Kapton film (maintained at three different temperatures).

The van der Pauw technique⁴ was used to measure the electrical properties of Hall resistivity, carrier density, and Hall mobility of the ITO-coated disks and the OSR before and after flight. No changes in these properties were observed for any of the samples.

Optical constants and coating thicknesses of the ITO-coated disks were measured by ellipsometry before and after flight. No changes were observed.

The specular reflectivity of the OSR after flight was measured in the range of 200 to 800 nm (using a Cary 17 spectrometer), and from 2 to 25 μm (using a Nicolet MX-1 Fourier transform infrared spectrophotometer). No differences in reflected intensity or in the spectral shape of the reflectivity were discernible among the two flight samples and a number of laboratory control samples.

To examine the ITO-coated Kapton films for changes in mass, 0.9-in.-diam disks punched from the samples were weighed. Comparison of the measured masses of the flight samples to those of disks punched from material kept in the laboratory showed no change in the masses of the films.

Taken together, these measurements lead to the conclusion that ITO films are not affected by the low Earth orbit atmosphere; furthermore, they indicate that ITO coating of Kapton will inhibit its erosion by atmospheric atomic

oxygen. One caveat must accompany this conclusion: laboratory studies show that the heating of conductive ITO coatings above 200°C in air results in their complete loss of conductivity. One expects that the heating of ITO in the oxidizing atmosphere of low Earth orbit would produce a similar result.

C. POLISHED NICKEL MIRROR

Observations of the surface erosion of a variety of materials raised the concern that the reflective surfaces used to line sunshields on orbital sensors might be affected in such a way as to increase scatter, or nonspecular reflection. Four samples of polished, chemically deposited ("electroless") nickel, supplied by Westinghouse Electric Corporation (WEC), were flown on STS-5. Sample 1 was mounted in position A53-C-UP; sample 2 was mounted in position A53-C-DOWN. Samples 3 and 4 were kept as laboratory controls.

Measurements of the scatter of the mirrors, as quantified by the bidirectional reflectance distribution function (BRDF), were made by WEC on all four disks, both before and after the flight exposure of samples 1 and 2. The light source used in their measurements was a 5-mW helium-neon laser (6328 Å). The angle of incidence of the laser beam on the samples was 10° from normal.⁵

Table 4 shows the results of postflight measurements of the BRDF value at a 20° angle of incidence. Changes in samples 3 and 4 are subjective, because the substrates were not flat enough for a reliable measurement.⁶

Visual observation under high-intensity illumination supports the results in Table 5. Low-magnification electron micrographs clearly show differences between the exposed and unexposed areas of the sample.

The surfaces of the nickel mirrors were chemically analyzed by x-ray photoelectron spectroscopy (XPS). The nickel XPS spectra of flight samples 1 and 2 show the presence of only oxidized nickel, while the spectra of laboratory samples 3 and 4 contain signals for both oxidized and metallic nickel. The oxide layer on the flight samples is thus thicker than that on the laboratory samples, since the substrate metallic-nickel signal is not visible in the spectra. Given the escape depth of the electrons involved in the analysis and the geometry of the spectrometer, one can estimate that the oxide

Table 4. Postflight BRDF Summary

Sample No.	Location	Preflight BRDF, 20° [W/W-Sr]	Postflight Increase (Decrease) at 20°
1	up	1.3×10^{-4}	6.4/1
2	down	1.5×10^{-4}	17/1
3	control	4.8×10^{-4}	2/1
4	control	7.1×10^{-4}	(2/1)

on the laboratory samples is on the order of 10 Å thick; on the other hand, the oxide on the flight samples is more than 30 Å thick, which is the sampling depth of the spectrometer.

This experiment has shown that the exposure of polished electroless nickel reflectors to the low Earth orbit atmosphere results in a significant degradation in performance, as measured by the BRDF of the surfaces. Surface analysis by x-ray photoelectron spectroscopy indicates that this degradation is the result of oxidation of the surface by the ambient atmosphere. It is of particular significance that the sample that was nominally shielded from direct atmospheric impingement showed a larger effect as measured by both XPS and BRDF. This is consistent with the observation that silver foils, flown on tray A53, showed more extensive oxidation on the "down" sample than on the "up" sample. This result shows that significant oxidation of the nickel surface can occur from atomic oxygen that has struck one or more spacecraft surfaces before reaching the nickel.

III. ORGANIC AND METAL FILMS

The purpose of this experiment was to determine the effects on organic and metallic films of exposure to atomic oxygen in low Earth orbit. The potential of atomic oxygen impingement to remove contaminants by an accelerated oxidative process, and the possibility of contaminants being transferred to other surfaces via reactive chemical sputtering, are two important mechanisms of contamination. This experiment was designed to measure simultaneously the degradation of various organic films as well as to detect sputtered material from these films by using Fourier transform infrared (FTIR) spectroscopy. Metal films were analyzed by nuclear backscatter and ion microprobe mass analysis (IMMA) to study effects of exposure to atomic oxygen as well as of possible metal atom sputtering.

A. EXPERIMENTAL PROCEDURE

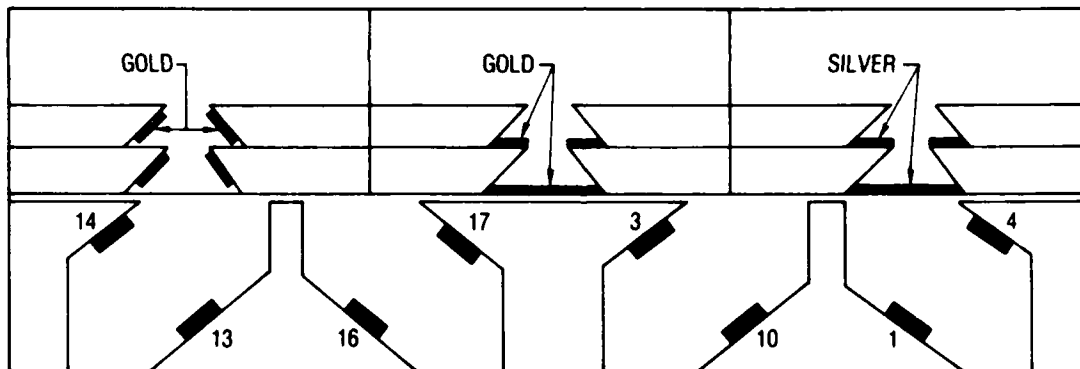
This experiment used a special fixture, a tray designed by Aerospace. Figure 2a is a photograph of the assembled tray with the cover removed, and Fig. 2b is a schematic of this fixture showing how the films were layed out. A schematic showing how the tray functions is presented in Figs. 3a and 3b, for organic and metal films, respectively.

A beam of atomic oxygen, collimated by slits in the tray cover, impinges on a germanium FTIR plate that contains a film. Close to the sample is another FTIR plate used to catch any sputtered material. Four of these sample-witness plate pairs (Figs. 2a and 2b, foreground) were used, and they occupied one half of the fixture. The other half of the fixture (Figs. 2a and 2b, background) contained the metal film experiment, wherein an oxygen beam, collimated by slits in the tray cover, strikes metal film targets and sputters metal atoms to the side collectors; here three such assemblies were used.

The organic films, prepared by the use of solvent airbrush techniques, were a hydrocarbon grease, a methyl silicone grease, and an epoxy. Kapton was a commercial film material. The identification and thickness ranges of these materials are presented in Table 5. The metal films used were gold, aluminum,



A



13 - KAPTON FILM
 16 - EPON 1001 RESIN
 10 - APIEZON L FILM
 1 - G-9042 SILICONE FILM

14, 17, 3, 4 - COLLECTOR PLATES

B

Fig. 2. The Aerospace Organic and Metallic Thin-Films Tray.
 (a) Photograph of the tray with the collimating cover removed.
 (b) Cross-sectional schematic of the sample layout.

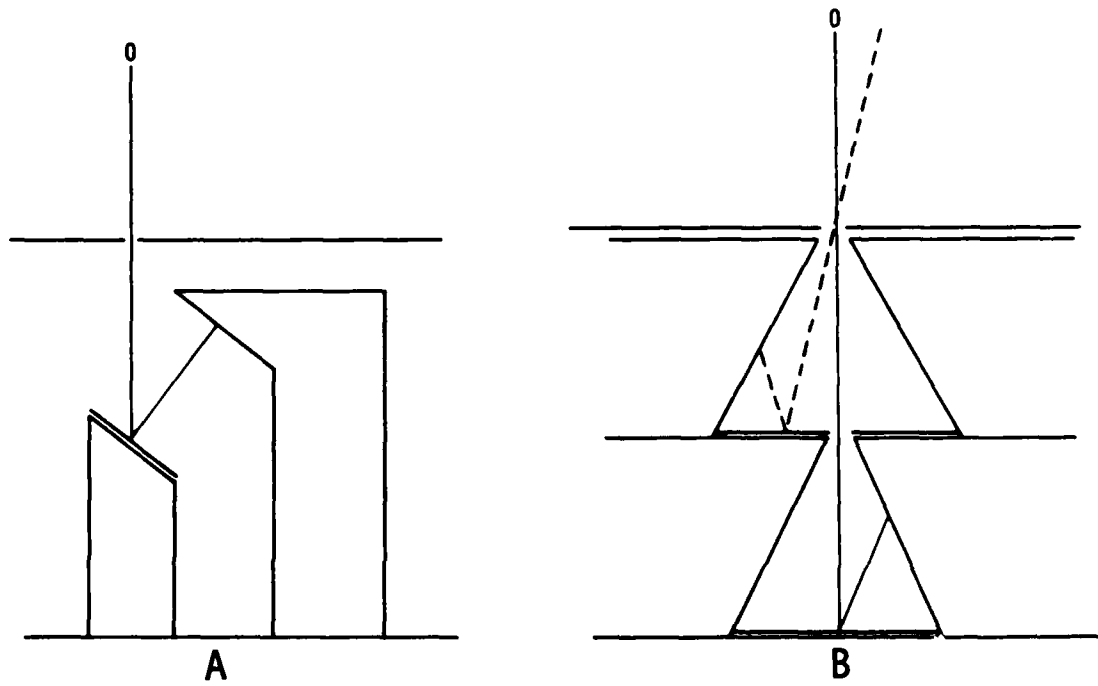


Fig. 3. Schematic of Tray Function. (a) Organic film configuration. (b) Metal film configuration.

Table 5. Materials and Results of Organic Thin Films

Sample	Thickness, mil	Result
Kapton sheet	0.5	eroded/pitted through
Apiezon L grease	0.1 - 0.2	removed
McGhan-Nusil G-9042 silicone grease*	1 - 2	oxidized and darkened
Epon 1001 epoxy**	0.2 - 0.3	eroded through

*The ZnO pigment was removed by filtration prior to coating.

**Cured with BDMA (benzyl dimethylamine).

and silver; these were vacuum deposited to a thickness of 1000 Å. In addition to this experiment, thicker silver foils were also placed in the Aerospace sample tray at location E (see Fig. 1b, above) for comparison with the results of this metal-sputtering experiment as well as with the results obtained from STS-5 with respect to oxide formation on silver foils.

B. RESULTS

The initial analysis of the metal film collectors using nuclear back-scatter indicated that roughly a monolayer ($10^{15}/\text{cm}^2$) of both gold and silver had been transferred to the side collectors from their respective targets. However, closer examination indicated that this layer was present on all faces of the collectors and was therefore the result of poor or inefficient masking of the parts during the metal coating process. Aluminum could not be detected on the collector because of background noise. Control samples run through the metal coating process showed the same contamination on their unexposed faces.

Interestingly, the silver target showed intense color changes as a result of exposure to oxygen. A dark-brown pattern was present at the point of maximum impingement and changed to a dark green; outward from the center, several different shades were observed. No unique oxide could be identified by ion microprobe mass analysis (IMMA) or x-ray analysis. Silver-coated collectors showed dark-brown areas, indicating that a large amount of oxygen atom reflection had occurred.

For the organic films the results are fairly clear. The 0.5-mil Kapton sample showed severe degradation and pitting. The FTIR spectra of protected and exposed areas show changes in the intensity ratios of the various bands. The 0.2-mil Apiezon film was essentially destroyed; FTIR spectra indicate that very little of the film remained. The 0.2-mil epoxy film was similarly degraded, as seen both visibly and by FTIR. The 1-mil film of methyl silicone grease was visibly intact, but darkened. However, FTIR analysis of the surface indicated that almost all of the hydrocarbon backbone had been removed and the remaining material was oxidized to a silicate. The FTIR spectra are shown in Figs. 4 through 15. Spectra were obtained by using both the attenuated total reflectance (ATR) and transmission modes for each sample. The most relevant spectra are presented for each sample.

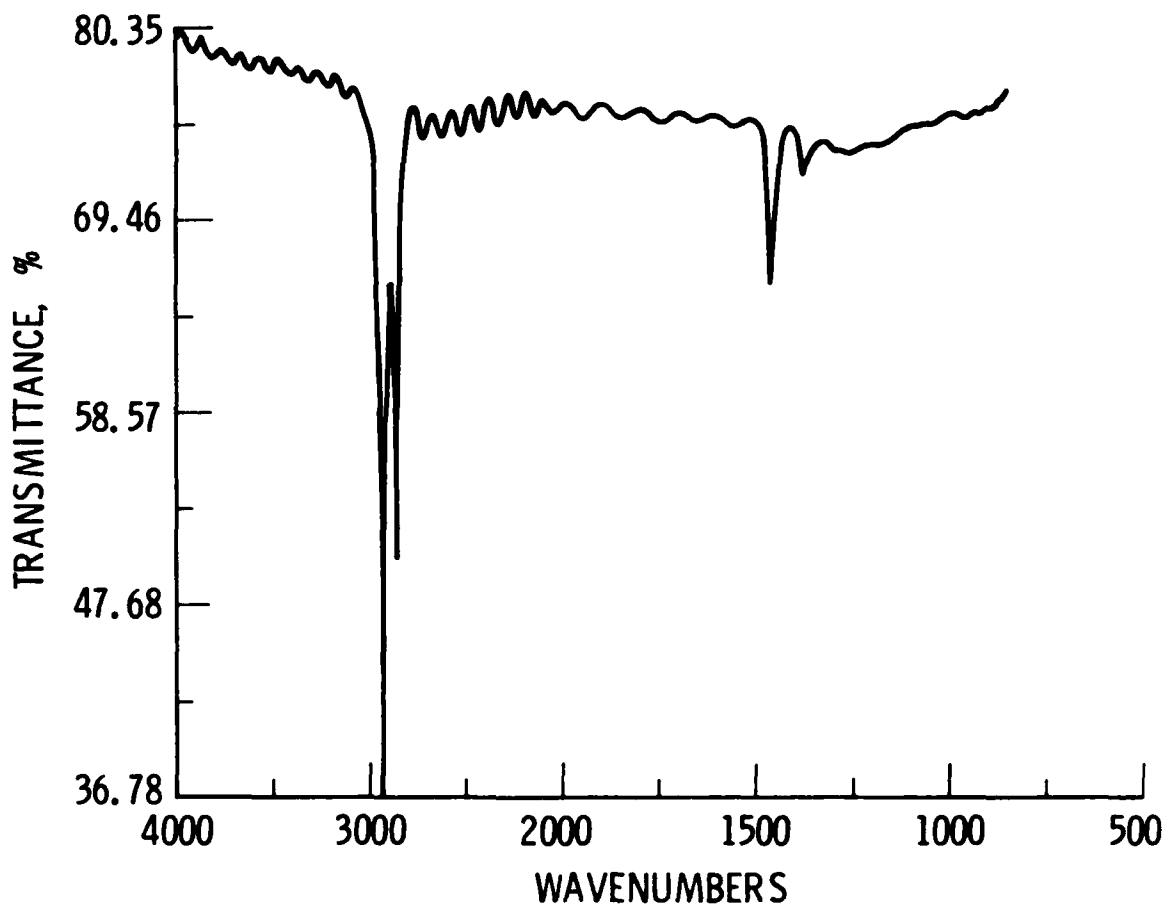


Fig. 4. FTIR Spectrum of Organic Thin Films: Preflight Apiezon (ATR Mode)

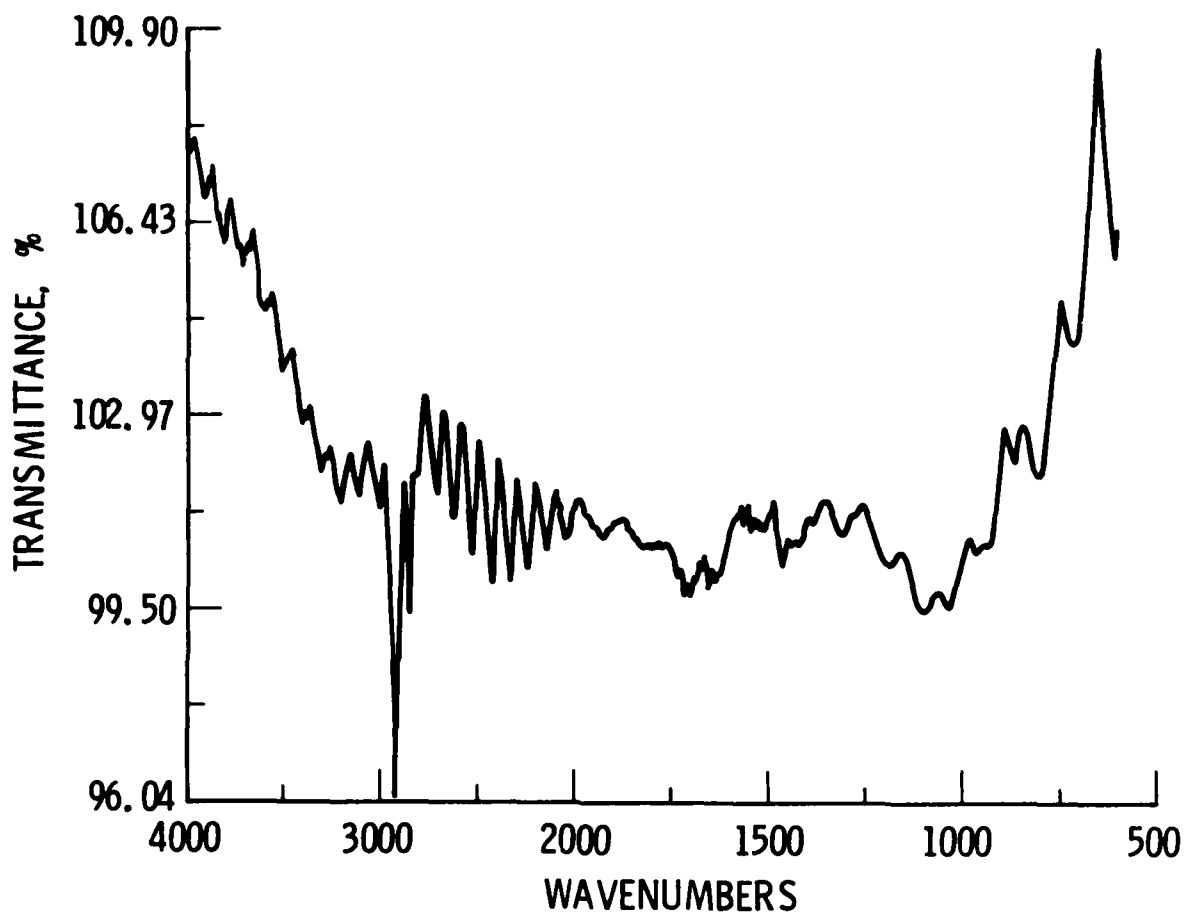


Fig. 5. FTIR Spectrum of Organic Thin Films: Postflight Apiezon (ATR Mode)

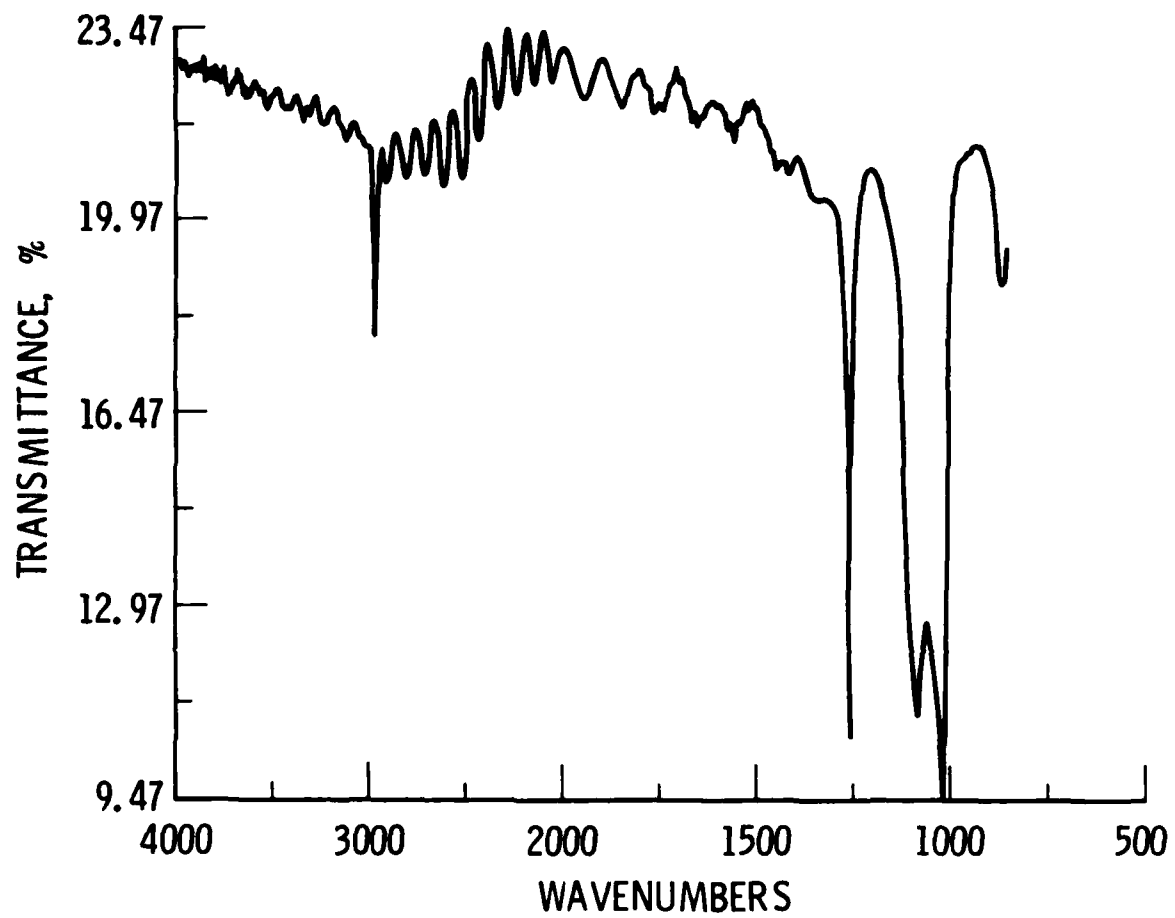


Fig. 6. FTIR Spectrum of Organic Thin Films: Preflight Silicone (ATR Mode)

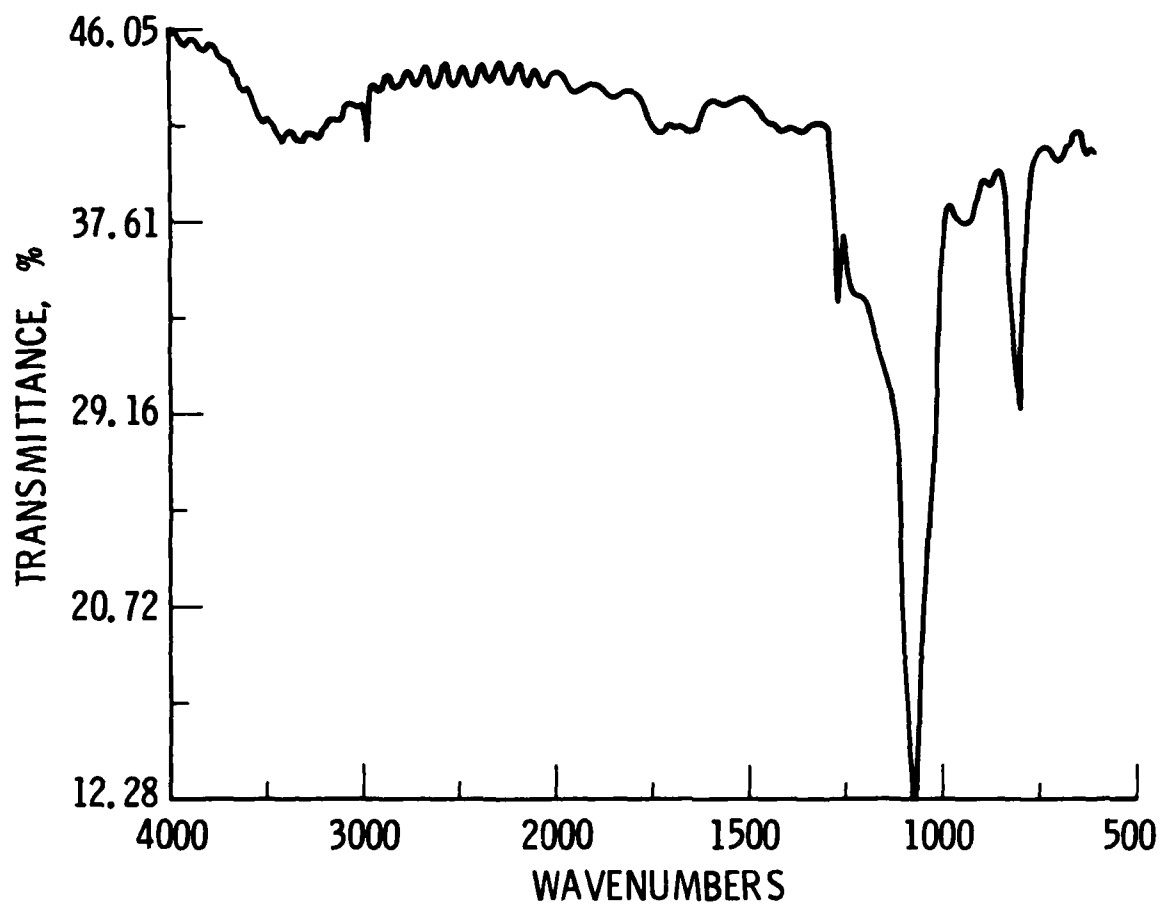


Fig. 7. FTIR Spectrum of Organic Thin Films: Postflight Silicone (ATR Mode)

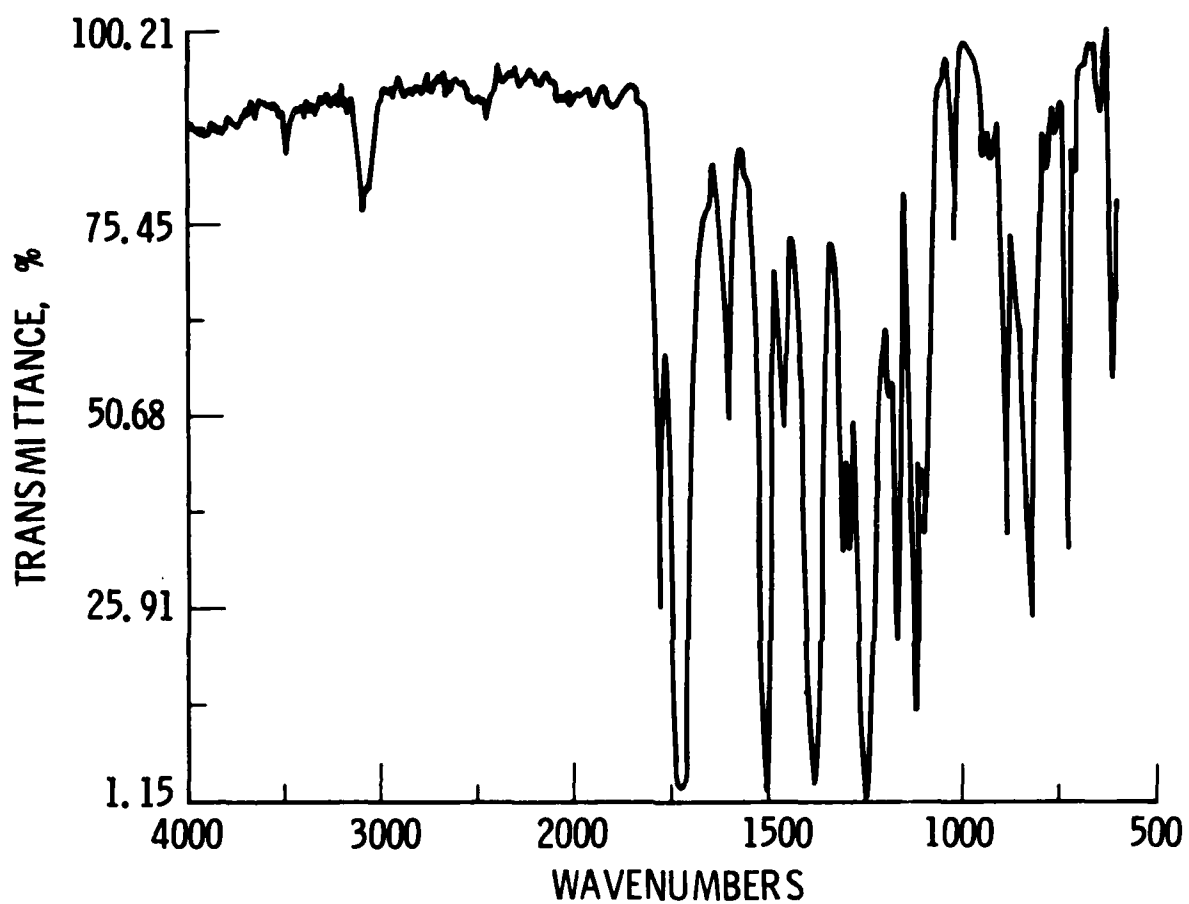


Fig. 8. FTIR Spectrum of Organic Thin Films: Kapton, Exposed Area (Transmission Mode)

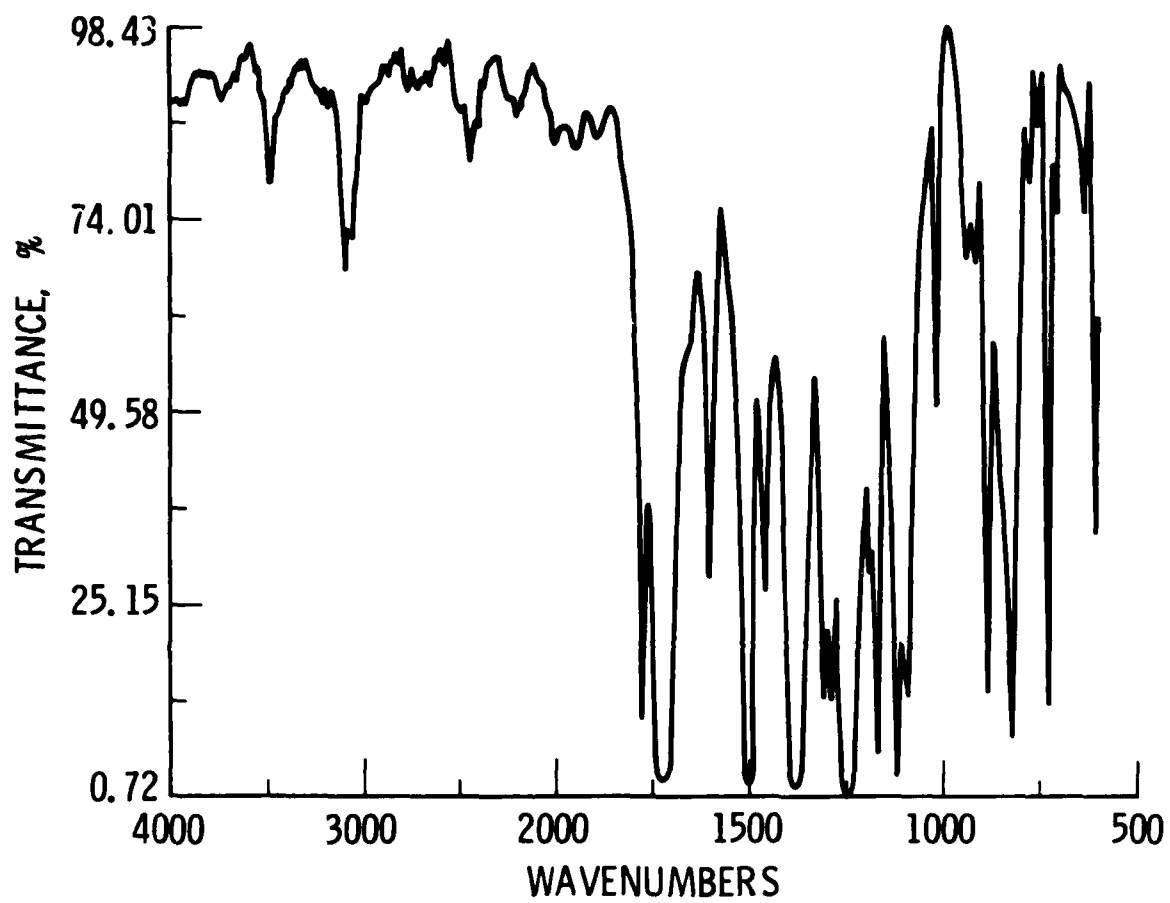


Fig. 9. FTIR Spectrum of Organic Thin Films: Kapton, Masked Area (Transmission Mode)

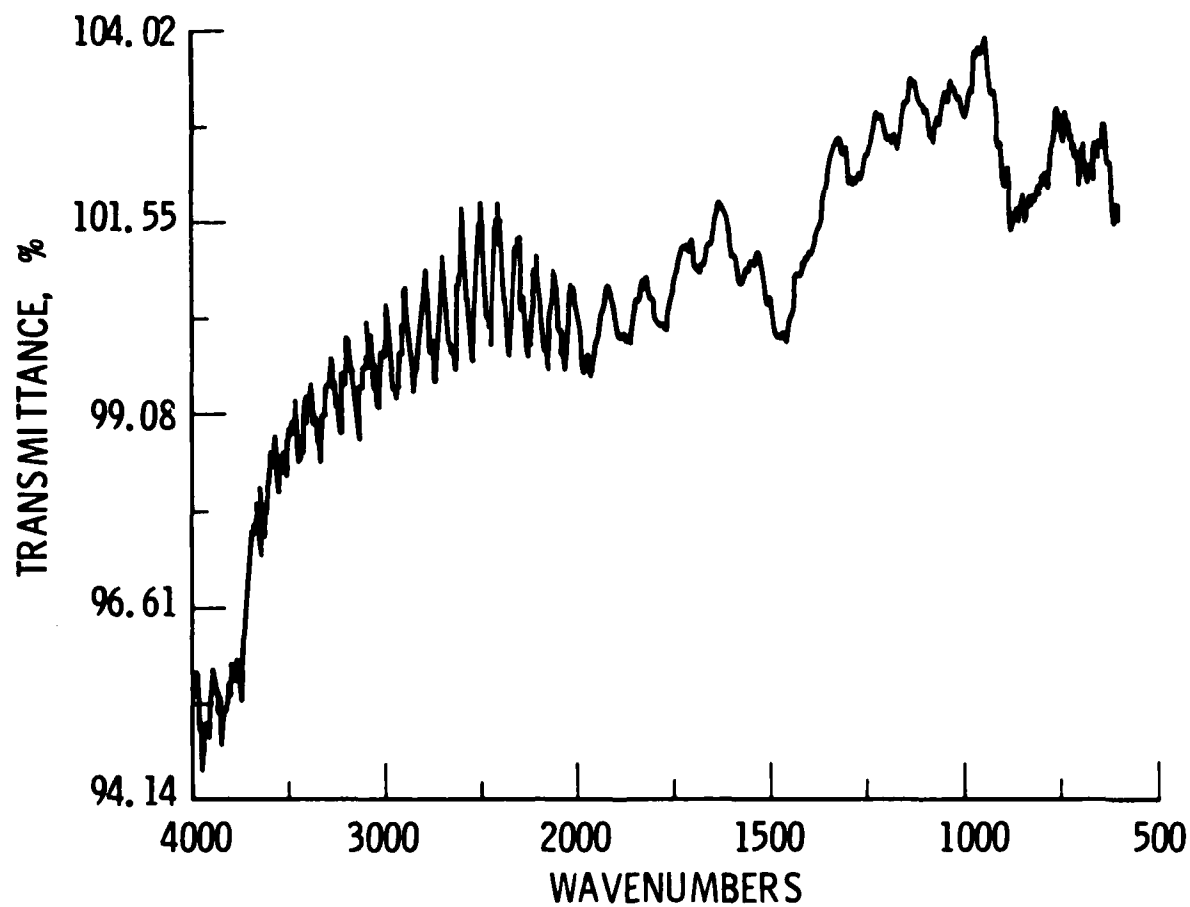


Fig. 10. FTIR Spectrum of Organic Thin Films: Epoxy, Exposed Area (Transmission Mode)

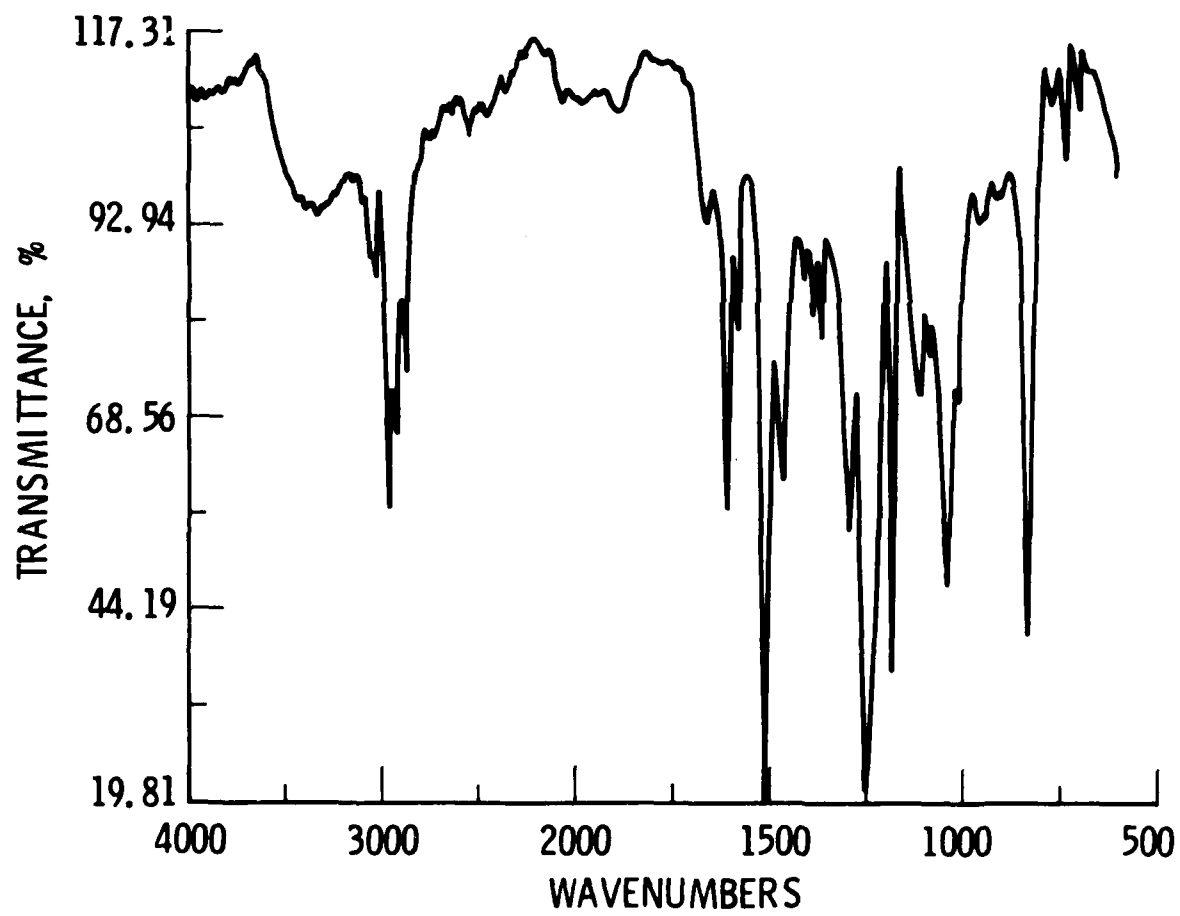


Fig. 11. FTIR Spectrum of Organic Thin Films: Epoxy, Masked Area (Transmission Mode)

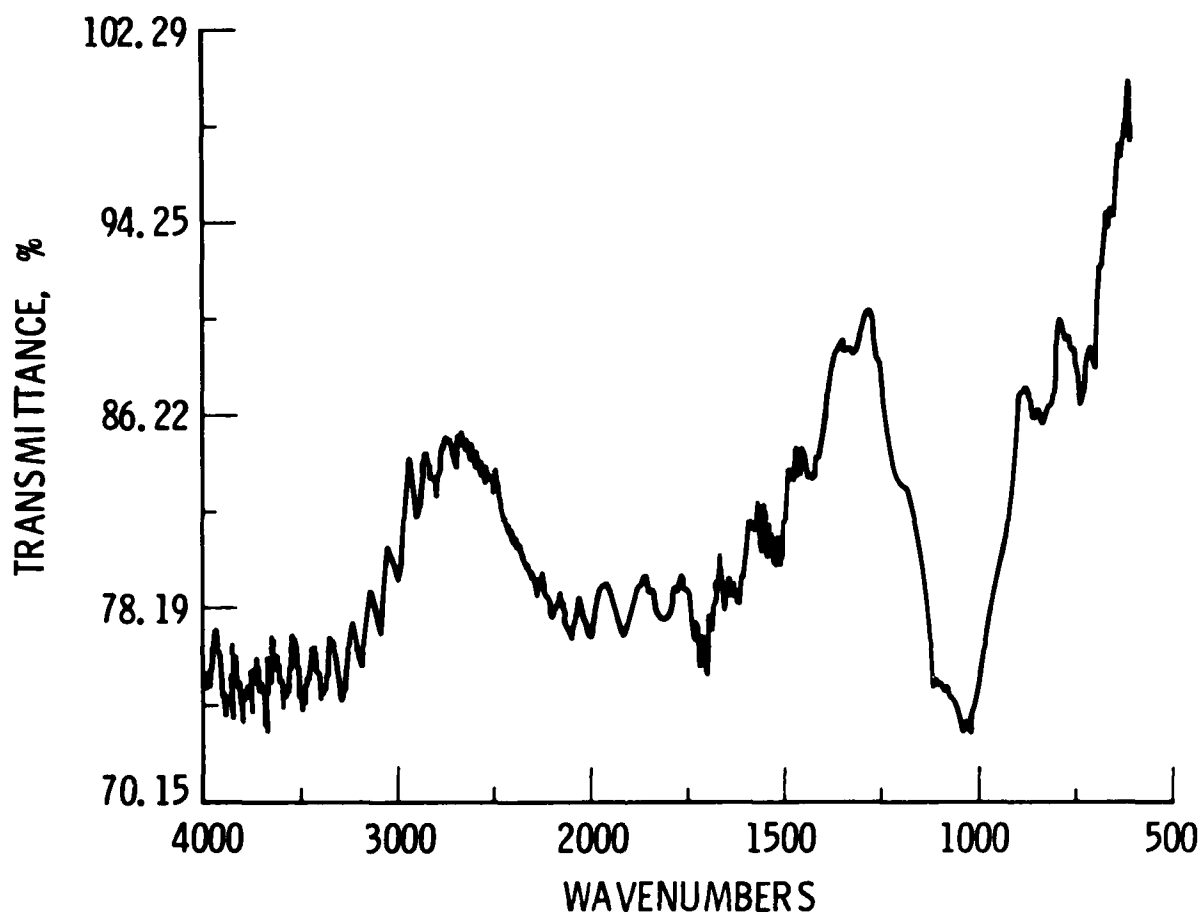


Fig. 12. FTIR Spectrum of Collector Plates: Silicone Collector Plate (ATR Mode)

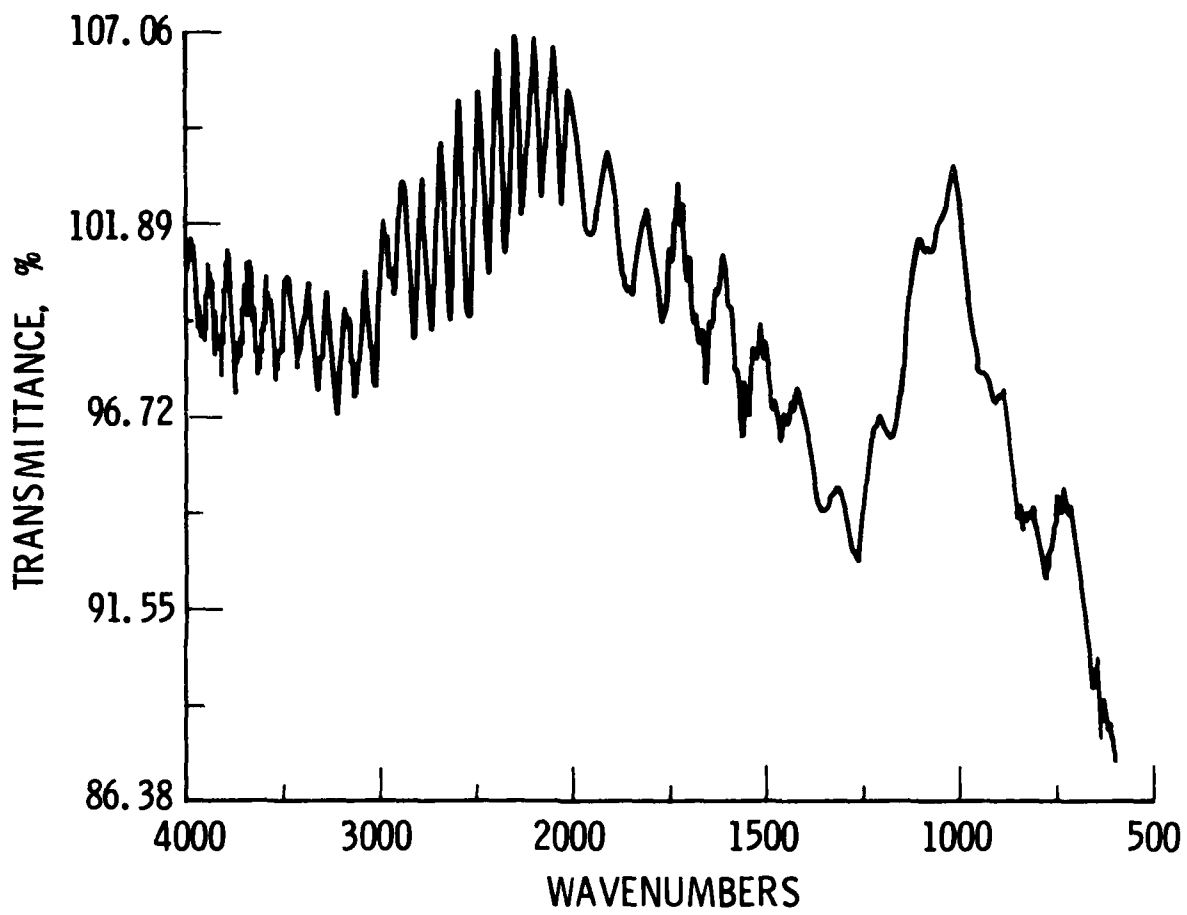


Fig. 13. FTIR Spectrum of Collector Plates: Kapton Collector Plate (ATR Mode)

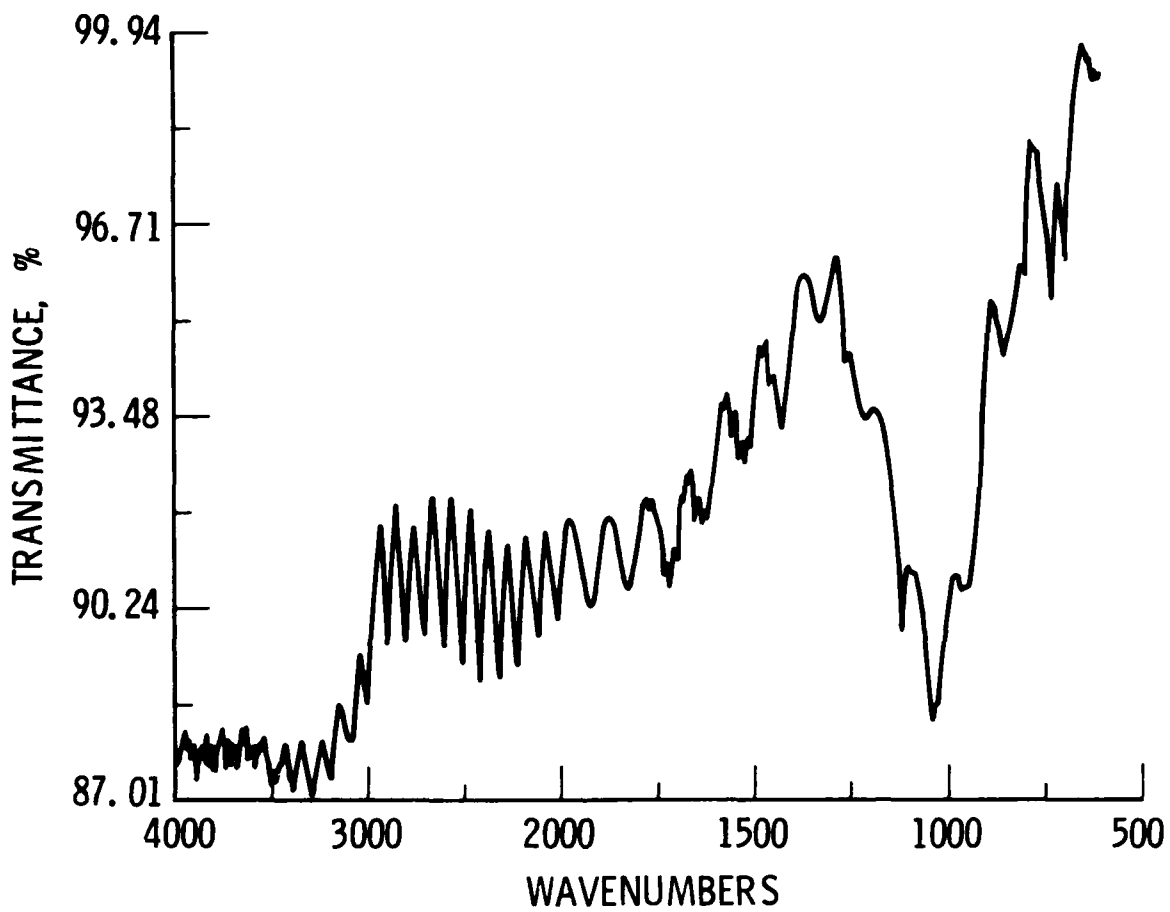


Fig. 14. FTIR Spectrum of Collector Plates: Apiezon Collector Plate (ATR Mode)

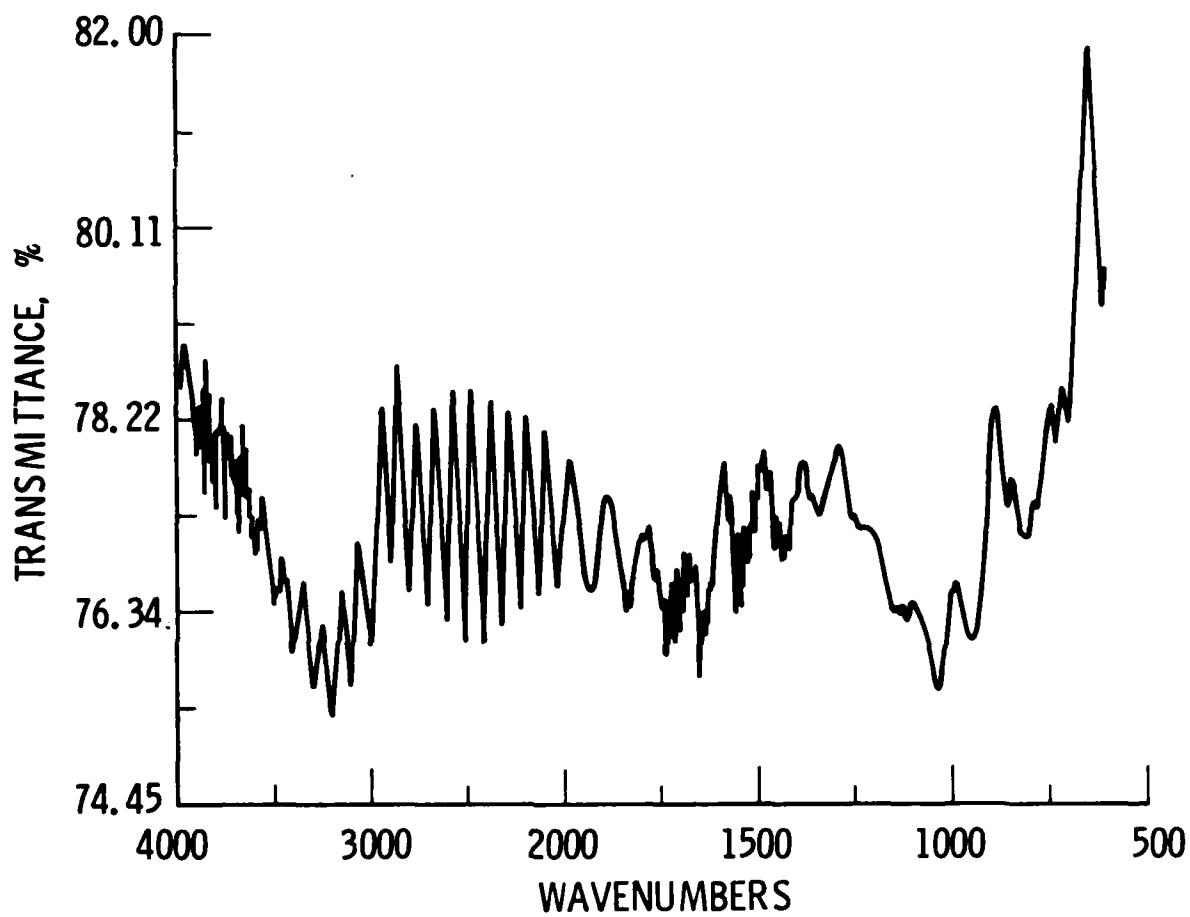


Fig. 15. FTIR Spectrum of Collector Plates: Epoxy Collector Plate (ATR Mode)

The collector plates do not lend themselves to such obvious interpretation. Material has been collected on at least three, and possibly all, of the plates. The amounts of material are very small and the FTIR spectra obtained are quite noisy. The plates opposite the Apiezon and methyl silicone grease samples had identical spectra. Very little, if any, material seems to have been collected opposite the Kapton and epoxy.

The silver samples were 99.97% pure in the form of foils 0.0127 mm thick. Identical samples were flown facing up and facing down, about one-half inch above the mounting plate for the experiment; these were identical to the silver foils also flown in the very same tray on STS-5. Three other silver samples, attached to the temperature-controlled film trays on STS-5, were also analyzed.

Results from STS-8 are shown in Table 6, along with the results previously obtained on STS-5 for comparison. Each result is an average of three ^{16}O depth profiles taken with an ion microprobe mass analyzer (IMMA). A typical profile for an "up" sample is shown in Fig. 16. The "down" samples did not generally show as sharp a step between the oxide and the silver but instead a more gentle drop in concentration, one consistent with more diffusion into the sample. On some samples the oxygen persisted to depths of over 3000 Å. The thicknesses in all cases were taken at the 50% intensity point on the profile. The oxide thickness is greater on the STS-8 sample, but the thickness is obviously not linear with oxygen atom fluence in this range of fluences. The down-facing samples are thicker in both cases; this is apparently caused by their reaction with oxygen atoms -- not from direct impingement along the velocity vector, but from scattering, reflection, or other unknown processes. Depth profiles taken in those areas of the silver foil masked from exposure to atomic oxygen showed less than 140 Å of native oxide thickness.

C. CONCLUSIONS

Metal sputtering, if it occurs at all, must have a yield of less than 10^{-5} . With respect to metal film stability, only the silver showed a tendency

Table 6. Thickness of Oxide Film on Silver

<u>Sample</u>	<u>Thickness, Å</u>	
	<u>Up</u>	<u>Down</u>
STS-5:		
A53	850	1060
2-75-7A	2900	1500
1-250-7A	2200	2600
2-250-7A	1700	2600
STS-8:		
E	1100	2100

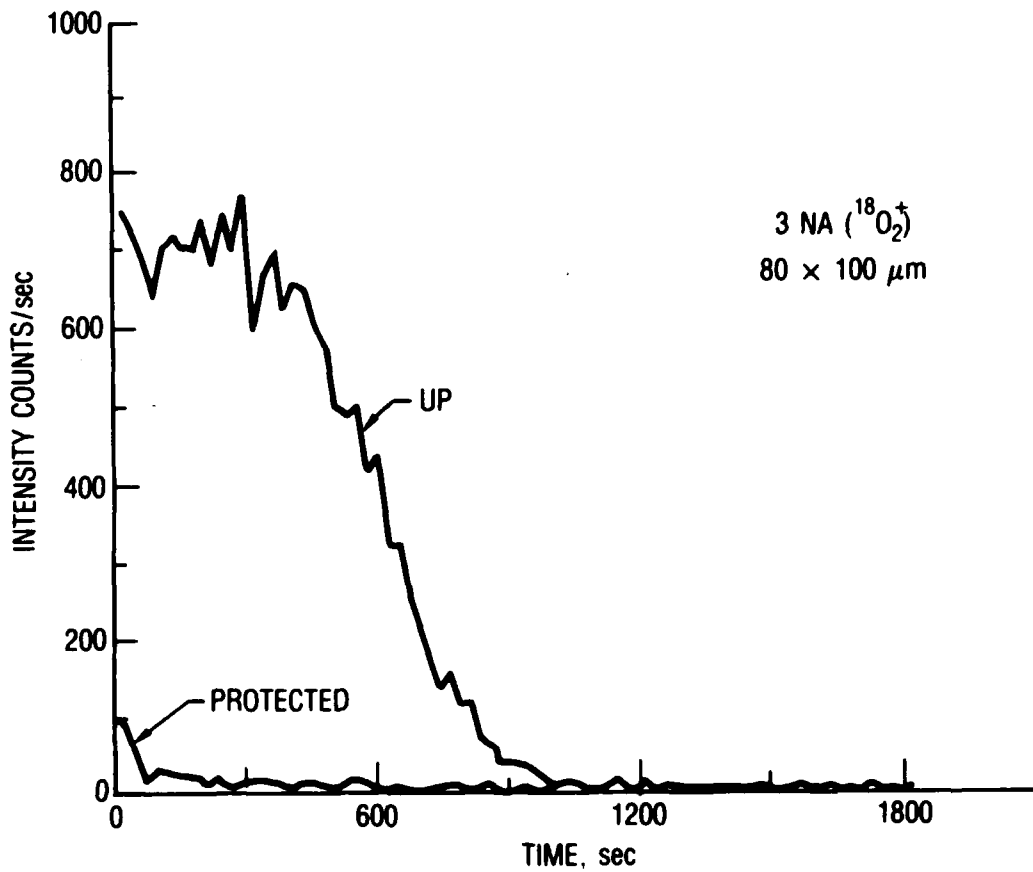


Fig. 16. Typical IMMA ^{16}O Depth Profile for an "Up" Sample of Silver

to oxidize. From both experiments, oxidation of the silver-coated specimens not directly exposed to the atmospheric rain indicates that oxygen atom reflection is a significant phenomenon.

From the organic and metal film experiment it appears that hydrocarbon contamination can be removed by atomic oxygen impingement, although silicone contamination will not be removed but will be altered and darkened by this exposure. Epoxies and Kapton will be eroded by atomic oxygen exposure. Material sputtered or transferred to another surface by atomic oxygen impingement was not observed. The nature of the contamination on the collector witness plates is unknown, but it would seem to be silicone related. The possibility that contaminants can be removed by reflected atomic oxygen cannot be dismissed; such removal may in fact be a significant mechanism by which materials are oxidized.

IV. STS-8 KEVLAR AND FIBERGLASS SAMPLES

A. EXPERIMENTAL PROCEDURE

Samples of plain, square-weave Kevlar 29 were placed in two locations in the EOIM experiment. A 1-in.-diam piece was inserted into the Langley disc sample tray (Fig. 1a), while a fourth tray, an Aerospace-fabricated aluminum holding fixture, housed a sample approximately 7-1/2 x 4-in. The Aerospace tray, 4 x 9 in. x 1 in. deep (see Fig. 17), also held a fiberglass sample (exposed) and O-atom-protected Kevlar and fiberglass samples on the back of the aluminum frame. The large Kevlar sample was held in the Aerospace tray at three different angles to the incident O-atom flux: at normal, 45°, and 60°. The fiberglass sample was positioned normal to the incident flux. Kapton tape was placed around the edges of the Kevlar and fiberglass samples to prevent the fabric from unraveling.

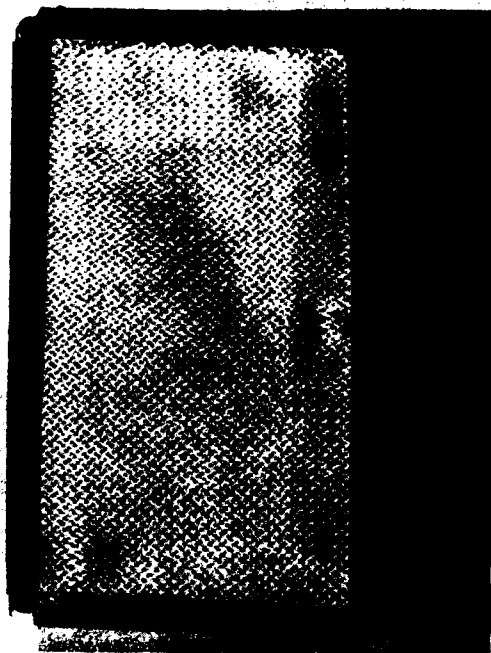
The purpose of mounting the Kevlar at different angles to the incident flux was to obtain different levels of O-atom exposure, thereby also obtaining physical-spectrophotometric properties as a function of dose for the Kevlar.

The two major concerns for the fabric were changes in mechanical strength and optical properties of the material as a result of O-atom exposure. Several analytical methods were chosen to measure any changes in mechanical strength or optical properties resulting from the O-atom environment.

B. RESULTS

1. MACROPHOTOGRAPHY AND MICROSCOPY

The surface sheen of the 1-in.-diam Kevlar sample was visibly dulled by O-atom exposure. The exposed areas of the Kevlar from the holding fixture were again obviously dull in appearance when compared with the unexposed areas (Fig. 18). The shiny areas were protected by the aluminum frame, as well as by Kapton tape placed around the Kevlar edges. There was no visible effect of O-atom exposure on the fiberglass sample.

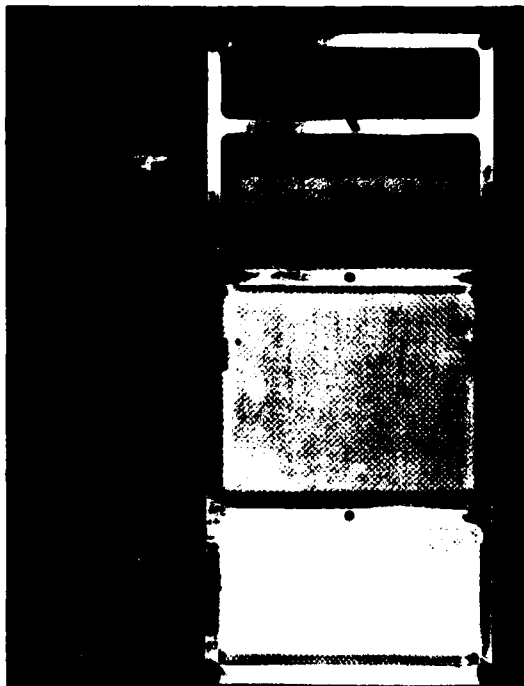


A



B

Fig. 17. Photographs of STS-8 Aerospace-Fabricated Holder for Kevlar and Fiberglass Samples (Preflight). (a) Front. (b) Back.



A



B

Fig. 18. Photograph of Kevlar from Flight Tray 2, Showing Surface Sheen Dulled by O-Atom Exposure. (a) Exposed. (b) Unexposed.

Samples of the exposed and unexposed fabric were viewed with the optical stereo microscope. Again, although the dull surface of the exposed Kevlar fibers was apparent, to the eye there did not initially appear to be any breakage or erosion of fibers, and the fiberglass sample did not at first reveal any visible change as a result of exposure to the O-atom flux. However, when the exposed Kevlar fabric was viewed in the scanning electron microscope (SEM), it was obvious that the surface had been eroded. This erosion probably gives the appearance of dullness or loss of sheen to the eye. There was no apparent change to the exposed fiberglass when it was viewed in the SEM.

A sample of the Kevlar fabric exposed under normal conditions was cross-sectioned and examined by means of optical and scanning electron microscopy in an attempt to see the extent of fiber damage. Most fibers on the exposed side appeared undamaged, with the possible exception of the outer surface of some of the fibers. In any case the erosion or damage does not appear to penetrate the fiber to any significant depth.

2. MECHANICAL TESTING

Mechanical testing of the Kevlar and fiberglass consisted of pulling samples to failure in an Instron model 1127 mechanical tester. Samples were tested from each of the three exposed areas of Kevlar and the one of fiberglass, as well as from unexposed laboratory and flight samples. Samples were mounted for testing in capstan-type holders to minimize clamping stresses. Fracture occurred at the center of the gage length in all samples.

The exposed Kevlar samples showed a 25 to 30% loss of strength compared with the unexposed Kevlar. The angle the Kevlar fabric made with the incident flux had little effect on the strength of the material. This was probably due to the nature of the fabric. The O-atoms strike normal to the fiber, damaging individual fibers regardless of their weave-exposure angle. Consistent with the fact that no damage could be detected via microscopy, the fiberglass sample exhibited no loss of strength as a result of the O-atom exposure.

3. SPECTROMETRIC MEASUREMENTS

Specular reflectance and absorption spectra of the pre- and postflight Kevlar and fiberglass samples were measured from 4000 to 400 cm^{-1} by means of the Nicolet MX-1 FTIR spectrophotometer. The absorption measurements were obtained on the fabric surfaces by pressing the fabric against a KRS-5 internal reflectance crystal and using the attenuated total reflectance (ATR) attachment to the FTIR. There were no significant changes in either the specular reflectance or absorption IR spectra between the exposed and unexposed samples of either the Kevlar or fiberglass.

Spectral hemispherical reflectance measurements were made with a Beckman 5240 spectrophotometer, while normal emittance values were obtained from measurements on a Gier Dunkle DB-100 spectrophotometer. The pre- and postflight solar absorptance α_s and emittance ϵ_N and ϵ_H (normal and hemispherical) values were obtained. Small changes due to O-atom exposure were noted in the absorptance and emittance values of the Kevlar. No significant changes were measured for the fiberglass sample.

C. CONCLUSIONS

The optical and mechanical properties of the Kevlar 29 fabric changed as a result of its exposure to the atomic-oxygen atmosphere at shuttle orbiter altitudes. The surface sheen of the Kevlar was noticeably dulled and the solar absorptance emissivity values decreased; no spectrometric changes were observed in the exposed fiberglass.

Mechanical testing revealed a 25 to 30% loss of strength in the Kevlar as a result of the O-atom exposure. The mechanical test data are presented in Table 7. Scanning electron microscopy revealed that the exposed fibers were eroded, though only the outer surface of the fibers appeared to be affected. However, this erosion was presumably insufficient in itself to cause the observed loss of strength. The mechanism causing fiber weakening is not known. The FTIR did not reveal any observable molecular change in the exposed fibers.

Table 7. STS-8 Kevlar Mechanical Testing Data

Sample*	Orientation	No. of Tests	Average Fracture Load, lb.	Breaking Strength, lb/in.	Normalized Strength, %
lab control sample	X (fill)	3	270	759	100
	Y (warp)	13	237	667	88
unexposed flight control sample	X	4	254	714	94
exposed sample (angled section at end)	X	3	202	568	75
exposed sample (angled section at center)	X	4	203	571	75
exposed sample (flat section)	X	6	187	526	69

* All samples have 8 strands.

Weave is approx. 22.5 strands/in. (warp and fill directions).

Breaking strength = $\frac{22.5}{8}$ (fracture load).

It has been suggested that the vacuum environment in space contributed to the loss in strength of the Kevlar, although the flight control sample exposed to the same vacuum and temperature history, but not to the incident oxygen flux, exhibited only a 6% loss of strength. Geometry should have prevented the oxygen atoms from reaching the sample.

Since we have only the one data point from which to extrapolate, there are insufficient data to determine the rate of change of the optical or mechanical strength properties in Kevlar with O-atom dose levels.

V. CARBON FIBERS AND GRAPHITES

A. SAMPLE DESCRIPTION

Carbonaceous materials were selected to ensure a meaningful representation of the range of structures and morphologies available. The large anisotropy of a single crystal of graphite is shown in Fig. 19. The materials consisted of five carbon fibers, one polymer fiber (Table 8), one bulk polycrystalline graphite, and a highly oriented pyrolytic graphite. The five carbon fibers ranged from a high-modulus, highly graphitic fiber (VSB 32) to a low-modulus, amorphous fiber (KGF 200). The one polymer-based fiber was a medium-modulus fiber having good fibril orientation. The bulk graphite was selected to represent the class of carbonaceous composites consisting of aggregates. The graphite had a bulk density of 1.86 g/cm and an open porosity of 16.7%, with essentially isotropic properties. Single crystals of graphite were represented by a highly oriented pyrolytic graphite.

B. EXPERIMENTAL PROCEDURE

The materials were prepared for the experimental trays in a manner that would enhance the observation of microstructural and morphological changes caused by oxidation via atomic oxygen (O). All six fibers were mounted in an epoxy resin and metallographically prepared in the transverse direction.

The axial plane of the bulk graphite sample was metallographically prepared and xenon-ion etched for exposure to atomic oxygen. To bring out the orientation of the graphite basal planes of the matrix phase in these materials, the polished surface was xenon-ion etched; this was also done for the a- and c-planes of the pyrolytic graphite. If the structure of the material is not overly refined, etch lines or laminae that indicate the graphite basal plane orientation will develop (Fig. 20).

C. RESULTS AND DISCUSSION

The changes after oxidation in the morphology and microstructure of the carbon and polymer filaments, bulk polycrystalline graphite, and pyrolytic graphite were qualitatively characterized by optical and scanning electron

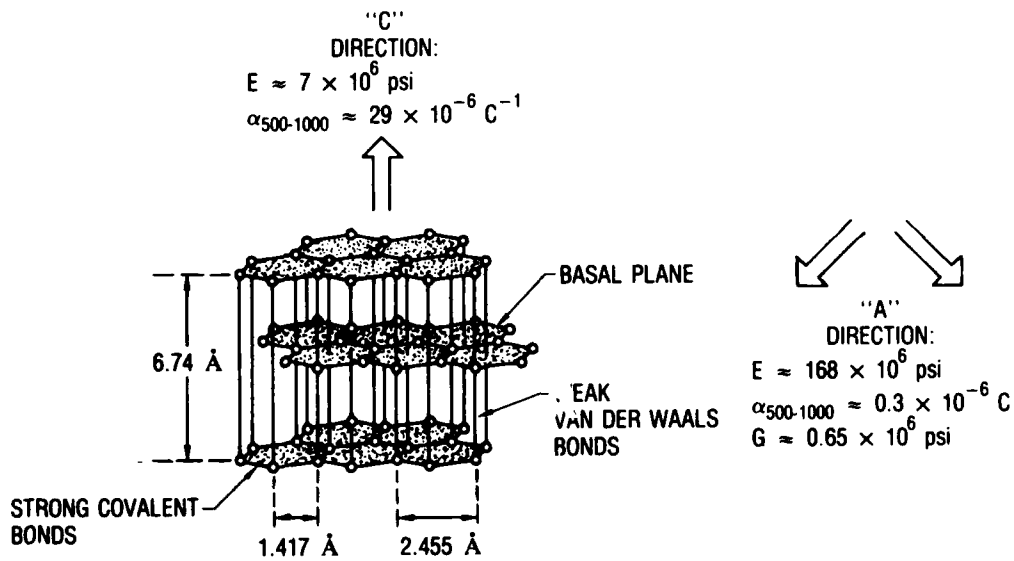


Fig. 19. Graphite Crystal Structure Showing Large Anisotropy. α is the coefficient of thermal expansion, E is the elastic modulus, and G is the shear modulus.

Table 8. Filament Property Data

Filament	Manufacturer	Precursor	Diameter, μm	Density, g/cm^3	Tensile Modulus, msi
KGF 200	Kureha	pitch	10	1.6	10
Thornel 300	Union Carbide	PAN	7	1.75	33
HM 3000	Hercules	PAN	8	1.83	50
VSB 32	Union Carbide	mesophase pitch	11	2.02	55
Kevlar	DuPont	polyamide	12	1.44	18
low-temp. PAN	Celanese	PAN	-	-	-



A

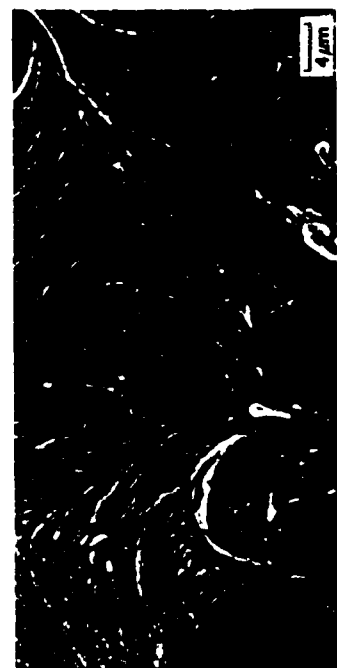


C

INTERMEDIATE
ORIENTATION

NORMAL
ORIENTATION

FILAMENT



B



D

Fig. 20. Photomicrographs of Xenon-Ion Etching of Polished Surface to Enhance Viewing of Graphite Basal-Plane Orientation. (a) As polished. (b) Ion etched. (c) Phenolic resin matrix system. (d) Pitch matrix system.

microscopy (SEM). However, the very slow rates of reaction for the carbonaceous materials prohibited quantification in this experiment. After exposure, the epoxy-based mounting compound used for the transverse sections of filament had oxidized at a faster rate than the filaments themselves, leaving the various filaments protruding above the oxidized plane of the mounting compound (Fig. 21). The changes in the filaments were a function of precursor-pitch, polyacrylonitrile (PAN), mesophase pitch, and polyamide, and the degree of graphitic order as reflected by the axial (longitudinal) tensile modulus. The carbon filament with an amorphous structure, KGF 200, appeared to have the least amount of in-depth oxidation (Fig. 22). The axial plane (transverse surface) was pitted with pores of varying shape and size which resulted from the oxidative attack of existing micropores; these micropores are present in amorphous carbons as a result of their low density, 1.6 g/cm^3 , compared to the density of a single crystal of graphite, 2.25 g/cm^3 .

The extent of surface and in-depth oxidation was found to decrease with increasing tensile modulus and density for the PAN-based filaments (Figs. 23 through 25). The low-temperature PAN with the lowest tensile modulus also had the greatest surface, transverse and longitudinal, and internal oxidation of the three PAN filaments. The appearance after oxidation suggests the fibril structure of PAN filaments which has been proposed by many researchers⁷ (see Fig. 23). The degree and extent of oxidative attack was reduced for the filaments having an intermediate modulus (Thornel 300, Fig. 24), and even more so for the filament having a high modulus (HM 3000, Fig. 25). The Thornel 300 filament also had a fibril appearance after oxidation. However, as this structure became more refined, resolving the fibrils became more difficult because of the smaller interfibril spacing (as in the high-modulus HM 3000 filament).

Another observation of the oxidative structure of the HM 3000 filament was that resistance to oxidation of the center core of the filament was apparently higher than that of the outer annulus (Fig. 26). Under more severe conditions, with flowing air at atmospheric pressure and a temperature of $\sim 3900^\circ\text{C}$, the outer annulus was oxidized away, leaving the resistant center core (Fig. 27).

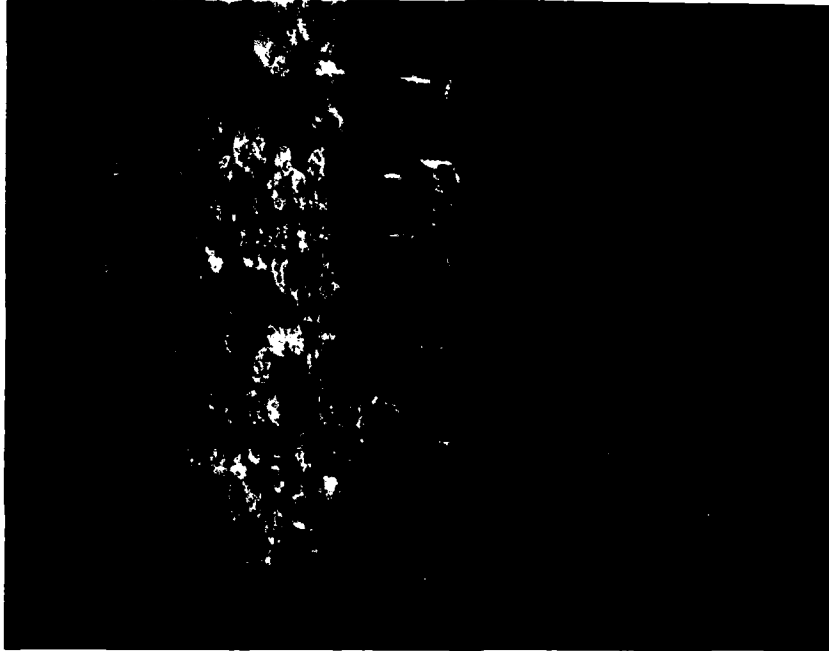


Fig. 21. Scanning Electron Micrograph of Mounted Carbon Filaments in Cross Section. Filaments protrude above oxidized plane of mounting compound.

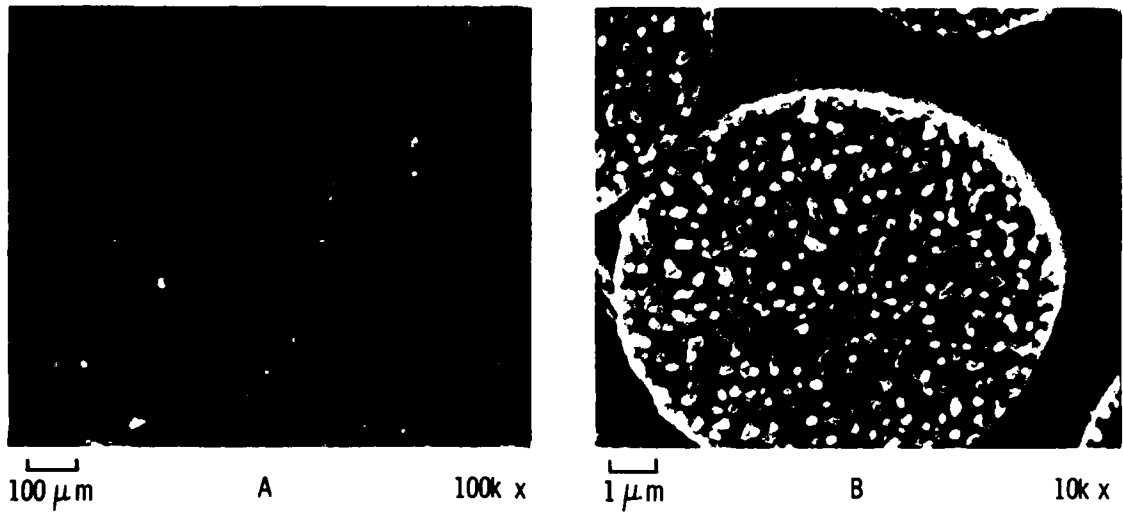


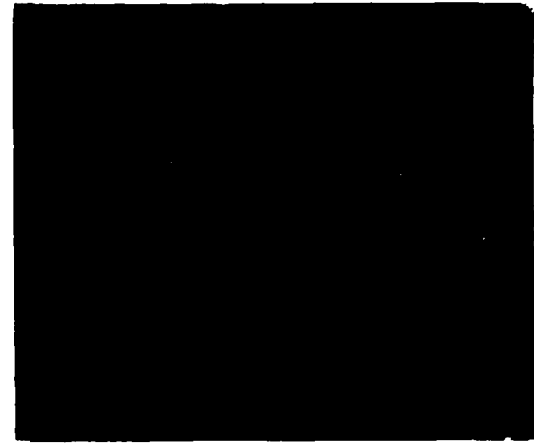
Fig. 22. Scanning Electron Micrographs of KGF 200. (a) Preflight.
(b) Postflight.



1 μm

A

10k x



1 μm

B

10k x

Fig. 23. Scanning Electron Micrographs of Low-Temperature PAN.
(a) Preflight. (b) Postflight.

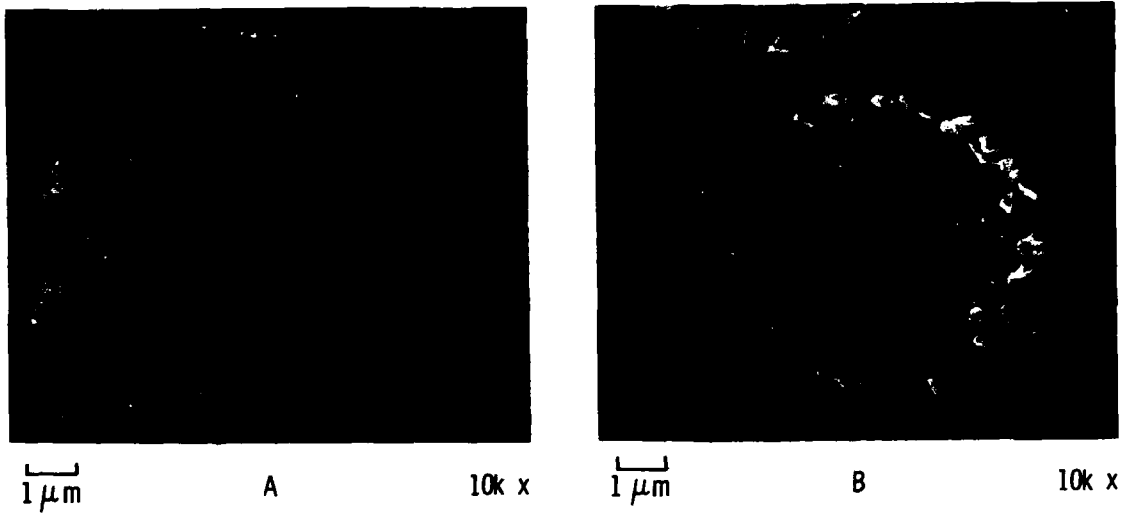


Fig. 24. Scanning Electron Micrographs of Thorne1 300. (a) Preflight.
(b) Postflight.

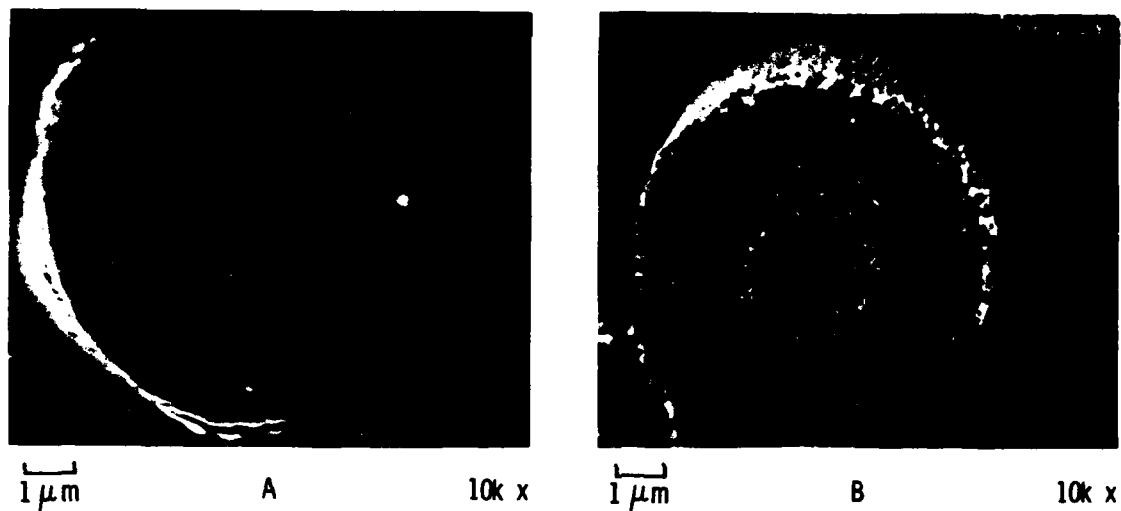
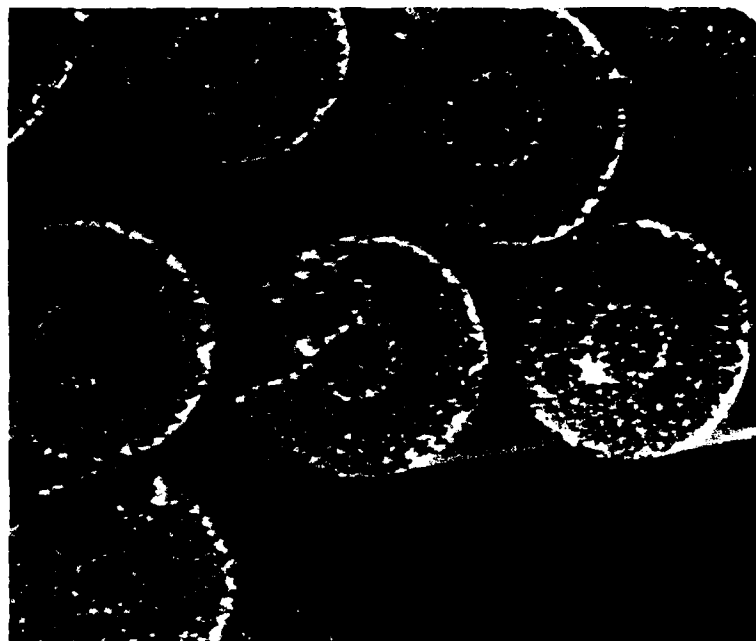


Fig. 25. Scanning Electron Micrographs of HM 3000. (a) Preflight.
(b) Postflight.



2 μ m

5k x

Fig. 26. Scanning Electron Micrograph of HM 3000, Showing Center Core Region

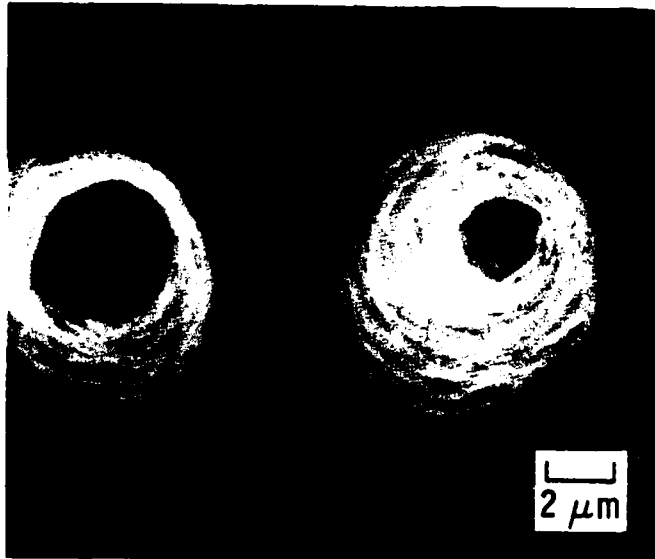


Fig. 27. Scanning Electron Micrograph of HM 3000 Filament after Oxidation in Air at Atmospheric Pressure and a Temperature of -3900°C

The post-oxidative characteristics of the transverse surface of the mesophase-pitch filament, VSB 32 (Fig. 28), were similar to those of the other high-modulus carbon filament, HM 3000. This fibril structure, which was common among the medium- and high-modulus carbon filaments, was also found in the medium-modulus filament made of Kevlar polyamide (Fig. 29). The development of this coarse fibril structure, a structure similar to that of the low-temperature PAN shown in Fig. 22, was not unexpected, considering the degree of alignment of the polymer planes required to achieve a tensile modulus of 18×10^6 psi.

Although the post-oxidative microstructural characteristics of the a- and c-planes of pyrolytic graphite were similar, the a-plane characteristics were an order of magnitude smaller. The fine conical structure after oxidation of the a-plane is shown in Fig. 30. The laminae shown in this micrograph of the a-plane clearly indicate the perpendicular orientation of the graphite basal planes to the plane of section. Micrographs of the c-plane before and after oxidation are shown in Fig. 31. Cross-sectional views of these conical features are shown in Fig. 32. The lack of a greater difference in the post-oxidative characteristics between the a- and c-planes was somewhat surprising, considering the large differences in the properties of the planes. The bulk polycrystalline graphite had microstructural features and coarse conical structures (Figs. 33 and 34) similar to those of the pyrolytic graphite. The microstructure suggested that oxidation resulted in the enlargement of micropores.

D. SUMMARY AND CONCLUSIONS

The results indicate that carbonaceous materials oxidize when exposed to atomic oxygen at the shuttle altitude. Although reaction rates for the carbonaceous materials could not be obtained, the epoxy was found to oxidize faster than the carbon filaments. The extent of microstructural changes in the materials depended on the degree of graphitic order and on the type of precursor. Carbons with an amorphous and highly graphitic structure, the extremes in structure, were the most resistant to oxidation as determined by the qualitative observations of microstructural changes in these materials. The relative reactivities at shuttle altitude are consistent with the relative reactivity observed from high-temperature oxidation.

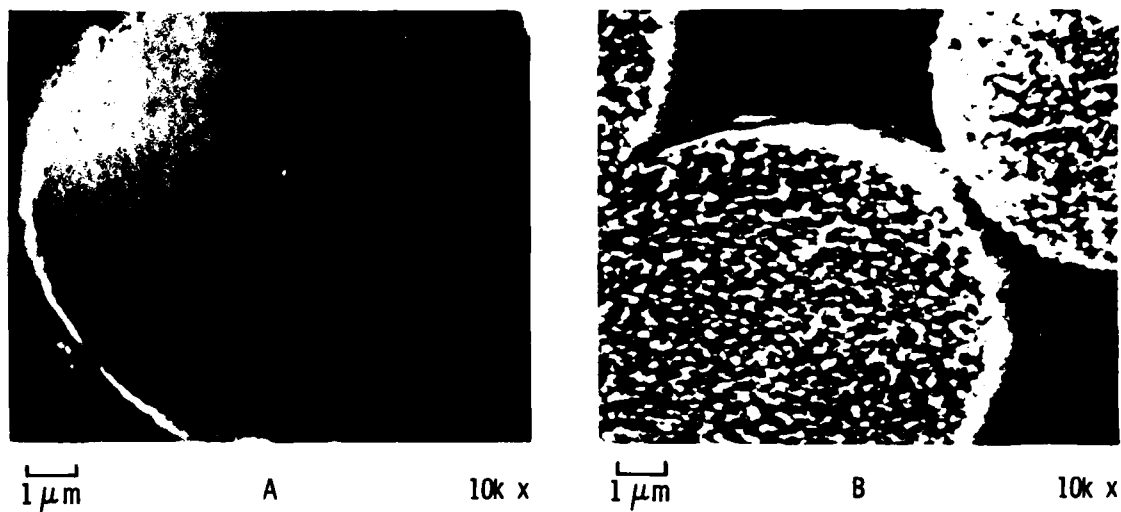
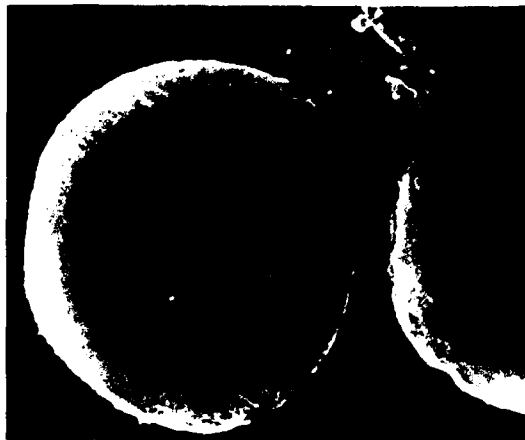


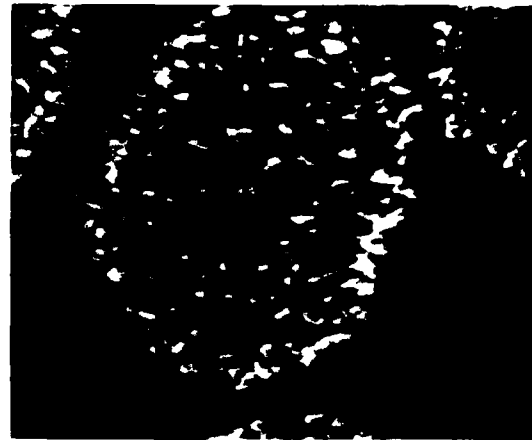
Fig. 28. Scanning Electron Micrographs of VSB 32. (a) Preflight.
(b) Postflight.



2 μm

A

5k x



2 μm

B

5k x

Fig: 29. Scanning Electron Micrographs of Kevlar Polyamid.
(a) Preflight. (b) Postflight.

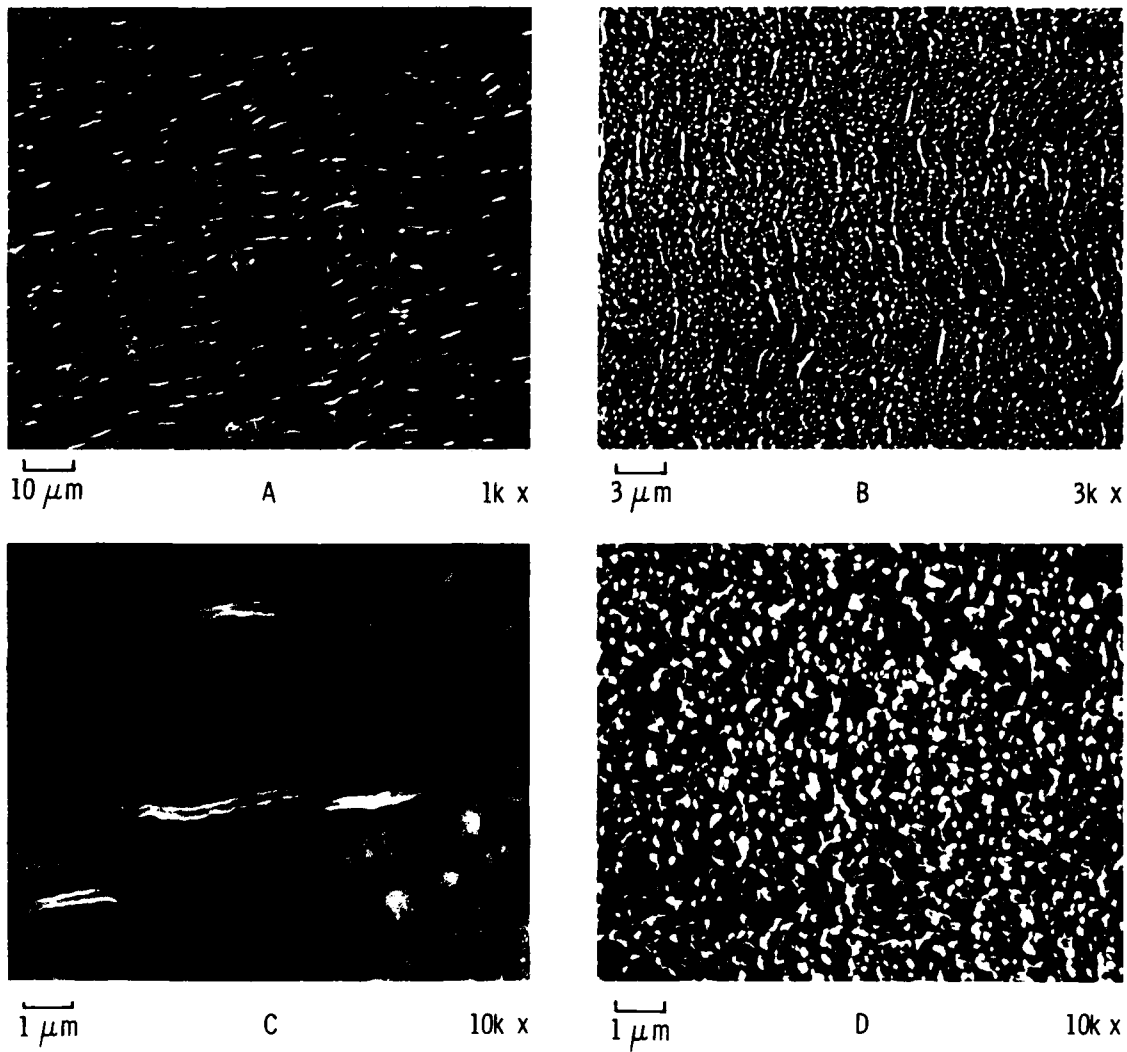


Fig. 30. Scanning Electron Micrographs of the A-Plane in Pyrolytic Graphite. (a) Preflight. (b) Postflight. (c) Preflight. (d) Postflight.

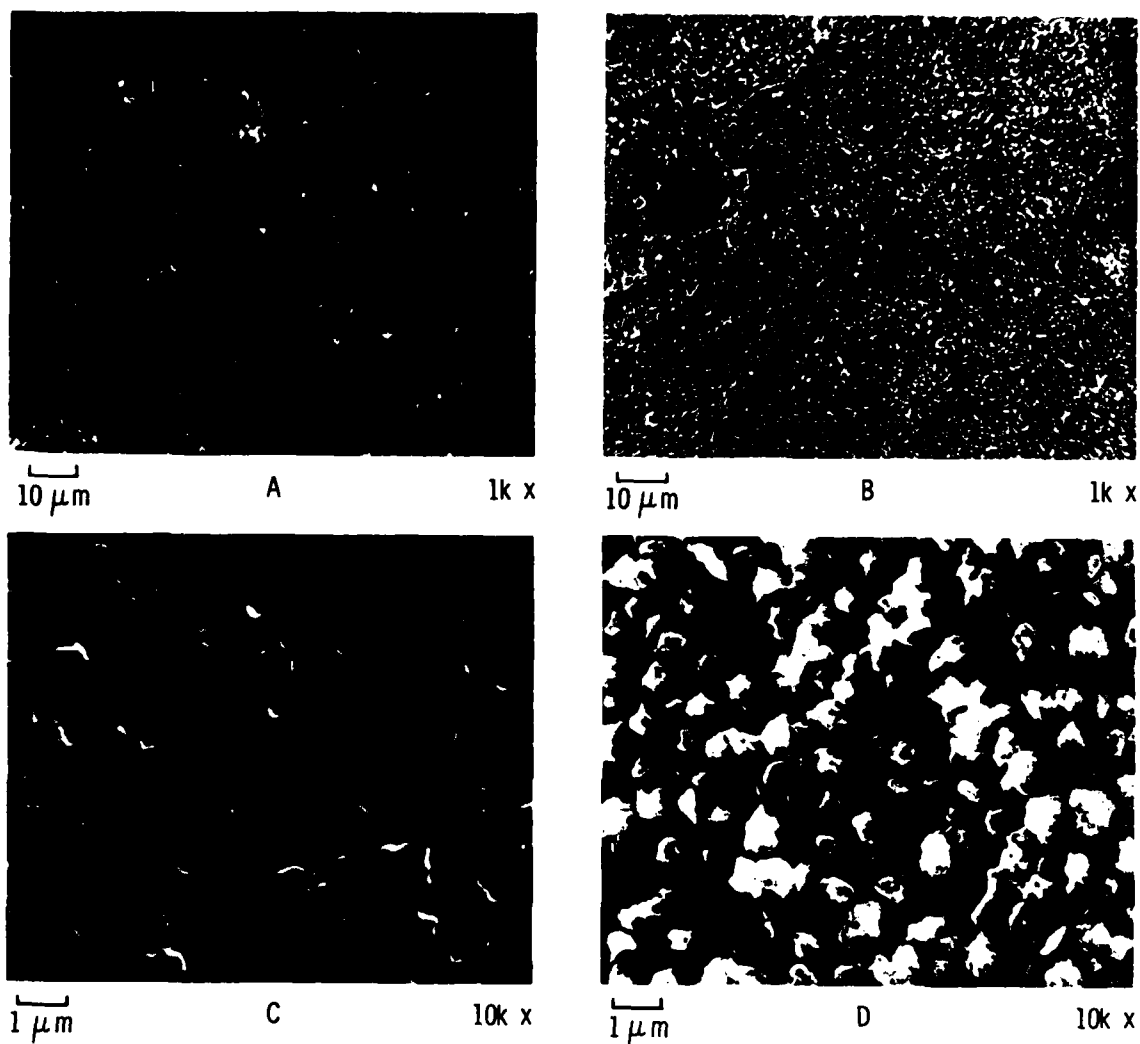
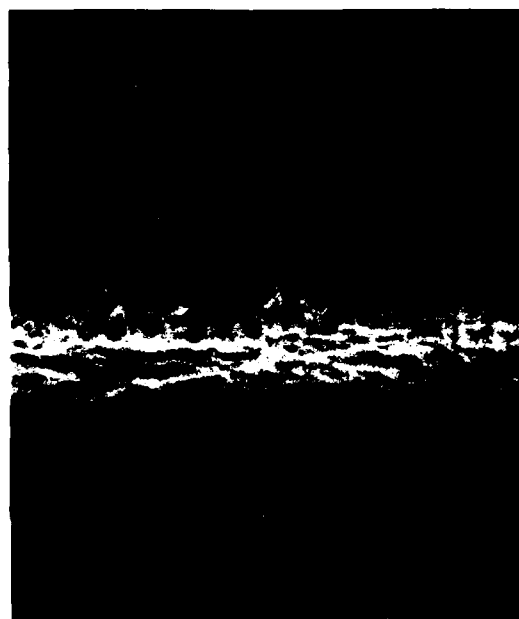


Fig. 31. Scanning Electron Micrographs of C-Plane in Pyrolytic Graphite. (a) Preflight. (b) Postflight. (c) Preflight. (d) Postflight.



100 μm

A



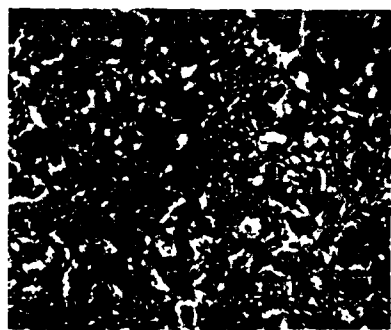
1 μm

B

Fig. 32. Scanning Electron Micrographs (Cross-Sectional View) of Conical Features in Oxidized Pyrolytic Graphite. (a) A-plane. (b) C-plane.



1 μm A 10k \times



3 μm B 3k \times



1 μm C 10k \times

Fig. 33. Scanning Electron Micrographs of POCO 5Q Polycrystalline Graphite. (a) Preflight. (b and c) Postflight.

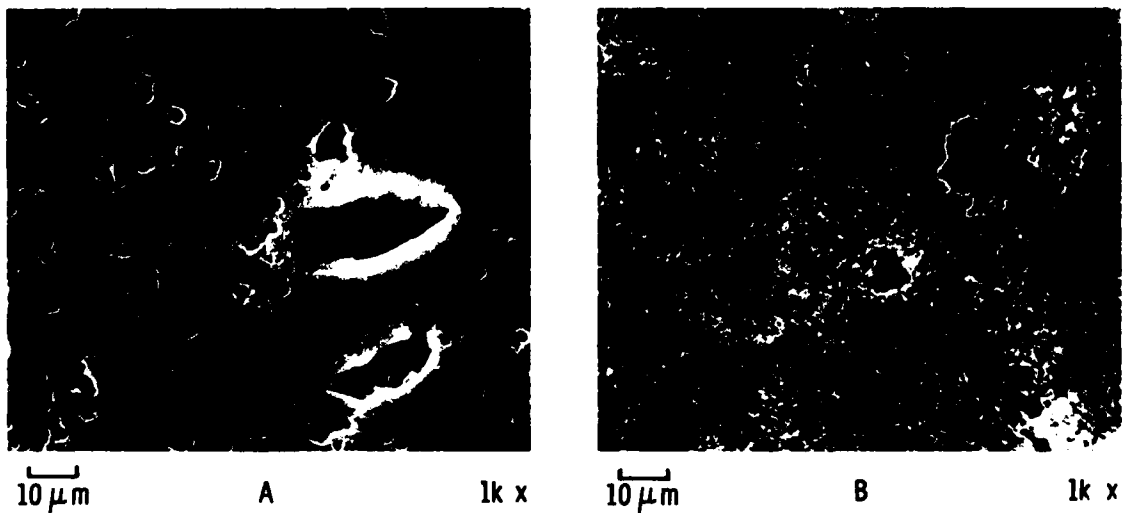


Fig. 34. Scanning Electron Micrographs of POCO 5Q Polycrystalline Graphite, Showing Changes in Micropore Diameters. (a) Preflight. (b) Postflight.

VI. HIGH-TEMPERATURE COATINGS

A. INTRODUCTION

Materials resistant to high temperatures are being developed for spacecraft applications. Coating materials and processes are necessary to provide thermo-optical properties that minimize heating caused by absorption of solar radiation, allow dissipation of heat, and also tolerate brief high-temperature excursions.

Of concern is the behavior of these materials in the orbital environment, as specific changes in their thermo-optical properties can cause problems. A number of candidate high-temperature coating and substrate materials are being considered for satellite thermal control; however, the effects of exposure to the shuttle environment are not well known. This is partly because, in previous space flights, samples of materials have not been given definite exposures and then retrieved for later examination. In addition, the exact conditions encountered on orbit are difficult to duplicate in the laboratory.⁸ Results from STS-4 are severe erosion of osmium and carbon films and changes in the appearance of silver films. Gold films, which appeared unchanged, indicated that sputtering was not the mechanism of degradation.⁹ There is thus reason for concern over the effects of this environment on other materials that may be used in the future.

The aim of this experiment was to expose samples of thermal-control coating materials to atomic oxygen bombardment in low Earth orbit and investigate any resulting changes in the infrared emissive and reflective properties and any correlated microstructural or textural effects.

B. SAMPLE DESCRIPTION

The coatings were applied to sample disks 1 in. in diameter and 0.125 in. thick. The disks were located in the Langley tray (see Fig. 1a, above). Various coating materials were applied to substrates of polished molybdenum (Mo), aluminum (Al), and titanium (Ti). The ten coatings investigated are described below.

1. Black rhodium on molybdenum (specular) - A rhodium (Rh) coating that was sputter-deposited to approximately 1 μm thickness from a Rh target onto a polished Mo substrate, using a vacuum sputtering unit (Edwards model 150B, under nitrogen at 0.3 mb). The coating had a shiny black appearance.
2. Black rhodium on Mo (matte) - Sputtered coatings of Rh on polished Mo, using conditions similar to (1); dull black in appearance.
3. Black iridium on Mo - Sputtered coatings of iridium (Ir) on polished Mo; black in appearance.
4. Black Cr on Cr on Mo - Mo substrates plated with Cr metal and coated with a high-emittance layer of black Cr.
5. Rh foil on aluminum - Highly reflective Rh foil applied to an Al disk by means of an adhesive.
6. Ir foil on Al - Same as for (5), but with reflective Ir foil.
7. Polished Mo - Disks of polished Mo.
8. KAT glass - Molybdenum sealing-glass composition coating, formed by sol-gel processing and doped with cobalt (Co) as a dark coloring agent, on a Mo substrate.
9. Ti/"tiodized" CP - Titanium anodized coating on a pure Ti substrate (a proprietary process, analogous to anodizing for Al, that consists of the electrolytic formation of a thick Ti oxide layer on Ti).
10. Ti/"tiodized" alloy - "Tiodized" coating on a Ti alloy (Ti-6Al-4V) substrate.

C. EXPERIMENTAL PROCEDURE

Two identical sets of samples were prepared; one set was flown and the other served as a control. Samples were photographed both before and after flight. To assess quantitatively the changes in the absorption and reflection properties of the samples, measurements of the infrared reflectivity in the 4000 to 500 cm^{-1} (2.5 to 20 μm) region were made before and after flight, using a Nicolet Fourier transform infrared (FTIR) spectrophotometer. Specular reflectance was measured, with the incident beam at 10° off normal.

Surface composition analysis and depth profiles were studied by means of a scanning Auger microprobe (SAM), and surface morphology was examined with a scanning electron microscope (SEM). The bonding of the coatings to the substrate was also examined by means of a tape-peel adhesion test.

D. RESULTS

1. VISUAL OBSERVATION, PRE- AND POSTFLIGHT

Some visual changes were observed on comparison of the postflight and control specimens, mainly on the Ir, Rh, and black Cr coatings. This is summarized in Table 9. The gross visual changes noted were mainly an apparent clouding or fogging of the surface, or the formation of small holes in the coating. Changes were also observed in the IR spectra of the coatings as a result of exposure to atomic oxygen.

2. FTIR RESULTS

Table 10 summarizes the changes observed in the IR spectra of samples that had accompanying visual changes. Except for the black Cr coating, the "fogging" is seen to decrease the measured IR reflectance. This can be interpreted as either an increase in the absorption of the sample, an increase in the diffuse reflectance, or some combination of each. However, it is to be expected that an increase in texturing of the surface such as that caused under various conditions of sputtering can lead to increased absorptance.^{10,11} Total reflectance over the maximum solid angle would be necessary to account for any changes in absorption compared to those caused by diffuse reflectance, although the changes induced in the coated samples (as indicated by the appearance of fogging) would likely be associated with an increase in absorption. In the case of the exception where reflectance increased, it seems likely that this increase is caused by the formation of actual holes in the coating, which causes the reflective metal substrate to be exposed and thus increases overall IR reflectivity. The changes in the IR spectra listed in Tables 10 and 11 are an indication of the change in average reflectance over the entire IR range measured. No major changes in spectral shapes or new peaks resulting from the exposure were observed.

Table 11 summarizes the IR changes observed in the remainder of the specimens, which did not exhibit visual changes. Some decreases in reflectivity were noted in the last three samples in the table. The low value of the reflectivity of the KAT glass samples made it difficult to determine the

Table 9. STS-8 High-Temperature Coating Experiment:
Visual Observations

Sample No.	Description	Postflight	Control
1	black Rh on Mo (specular)	clouded	no change
2	black Rh on Mo (matte)	clouded	no change
3	black Ir on Mo	clouded	no change
4	black Cr on Cr on Mo	pinholes	no change
5	Rh foil on Al	no change	no change
6	Ir foil on Al	no change	no change
7	Mo (polished)	no change	no change
8	KAT glass	no change	no change
9	Ti/"tiodized" CP	no change	no change
10	Ti/"tiodized" alloy	no change	no change

Table 10. STS-8 High-Temperature Coating Experiment:
 FTIR Difference Spectra (4000 to 500 cm^{-1})
 for Samples Having Changes in Appearance

Sample No.	Description	Postflight Change in Average Reflectance, %
1	black Rh on Mo (specular)	-50
2	black Rh on Mo (matte)	-25
3	black Ir on Mo	-75
4	black Cr on Cr on Mo	+20*

*More reflective as a result of the exposed Mo substrate

Table 11. STS-8 High-Temperature Coating Experiment:
 FTIR Difference Spectra (4000 to 500 cm^{-1}) for
 Samples Having No Change in Appearance

Sample No.	Description	Postflight Change in Average Reflectance, %
5	Rh foil on Al	no change
6	Ir foil on Al	no change
7	Mo (polished)	no change
8	KAT glass	-5 to 10*
9	Ti/"tiodized" CP	-40**
10	Ti/"tiodized" alloy	-25†

*Low absolute reflectance (-0.5 to 1%)

**Aging effect similar in STS-8 and control - no exposure effect

†Contrast in difference spectra between STS-8 and controls - possible aging effect on controls

change in reflectivity. The Ti/"tiodized" (titanium anodized) (CP) sample showed similar spectral changes in both the control sample (over a six-month period) and the postflight sample. The changes in the coating may have occurred gradually over a period of time, perhaps because of moisture absorption. Spectral changes occurred in both the postflight and control Ti/"tiodized" (alloy) samples, but the changes were somewhat different, as is indicated when the pairs of spectra are subtracted. This shows that, while the control sample may have changed during storage, there are also signs that the flight sample was affected by exposure to atomic oxygen.

3. ADHERENCE TEST

The degree to which the coatings adhered to the substrates, both controls and postflight samples, was examined by a simple tape-peel test.¹² Adhesive cellophane tape was applied to the coatings, then was peeled off and examined to determine if the coating had debonded from the substrate. The results are summarized in Table 12.

It is also noted that no major changes in adherence were found as a result of exposure to the atomic oxygen environment, except for the case of the black Cr coating. The adherence of that coating, which contained numerous small holes, was much less after the exposure.

4. SAM AND SEM RESULTS

Observation of the pre- and postflight samples by means of scanning Auger microscopy (SAM) showed some effects of exposure to atomic oxygen. Polished Mo showed a higher concentration of oxygen on the surface of postflight samples than on preflight ones. Surface profiling was performed in the instrument by sputtering away surface material with argon-ion bombardment and repeating Auger analysis. Oxygen was detected for a longer time (i.e., to a greater depth) in the postflight (Fig. 35a) than in the preflight samples (Fig. 35b), indicating that the energetic O-atoms create a significant oxidized surface layer.

Black Cr samples, both pre- and postflight, had similar composition profiles under Auger analysis. The Mo/Cr/black Cr structure was evident from

Table 12. STS-8 High-Temperature Coating Experiment:
Adherence Test

Sample No.	Description	Postflight	Control
1	black Rh on Mo (specular)	good (some debris)	good
2	black Rh on Mo (matte)	poor	poor
3	black Ir on Mo	good (some debris)	good
4	black Cr on Cr on Mo	poor	fair
8	KAT glass	good	good
9	Ti/"tiodized" CP	good	good
10	Ti/"tiodized" alloy	good	good

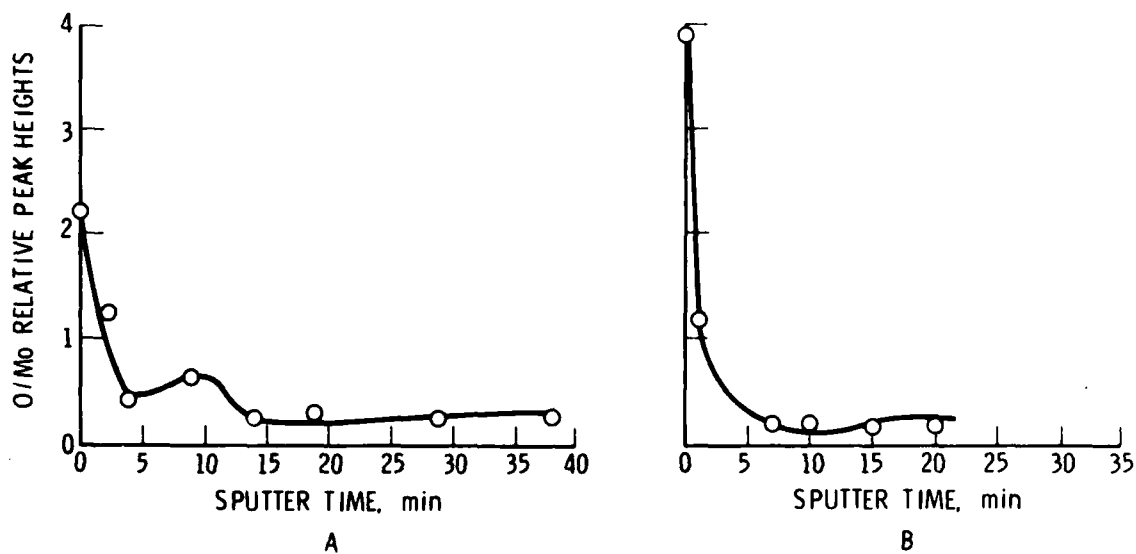


Fig. 35. Auger Surface Profiles of Polished Mo, Showing Oxygen Depth Profile. (a) STIS-8 flight sample. (b) Laboratory control sample.

the results. The coating appeared scaly and cracked into numerous, typically four-sided sections roughly several microns in diameter (see Fig. 36). The Auger analysis of the coating showed the material to be composed mainly of Cr and O, consistent with black Cr being a mixture of Cr and Cr_2O_3 (Fig. 37). Results were similar to SAM sputtering profiles obtained by Lampert¹³ on commercial black-Cr solar absorber coatings on nickel-plated copper, where further analysis by transmission electron microscopy (TEM) showed the coating to be composed of Cr_2O_3 particles interspersed with Cr particles. Regions in the cracks between the black Cr scales were found to be predominantly Cr (i.e., the metallic Cr undercoating), with small oxygen content. The Auger oxygen peak of the undercoating disappeared after brief sputtering, indicating the existence of only a superficial oxide layer. Comparison of the pre- and postflight black Cr oxygen content showed no significant differences attributable to atomic oxygen bombardment, although the microstructures of the black Cr scale had differed somewhat in appearance, probably because of differences in the surface finish of the substrates before coating.

An unusual debonding phenomenon illustrating the difference in adherence of the black Cr coatings in the pre- and postflight samples was observed in the SAM under electron beam bombardment. Under irradiation by the electron beam at 10 kV, some of the surface scales of the posttest samples were seen to debond spontaneously and appeared to fly off the surface, leaving an exposed area of the Cr undercoating (see Fig. 38). This was not observed in the pretest samples. It is believed that this may indicate charging of the surface scale, along with low adherence, so that the scales fly off as a result of electrostatic repulsion from the substrate. This would require the electrical contact between scale and surface to be poor. However, the bright voltage contrast due to charging, which one would expect to see in SEM images of the area, was not observed.

An interesting effect is the presence of a light-colored border along the edges of the surface platelets of black Cr, which is visible in areas where the platelets have debonded. This may indicate exposure of the Mo substrate, where O impinging through the crack has removed the Cr layer; however, it was not possible to probe the electron beam close enough to the base of the ledge



A 40 x



B 100 x

Fig. 36. Photomicrographs of Mo/Cr/Black Cr Sample, Showing Cracking and Scaling Caused by Exposure. (a) STS-8 flight sample. (b) Laboratory control sample.

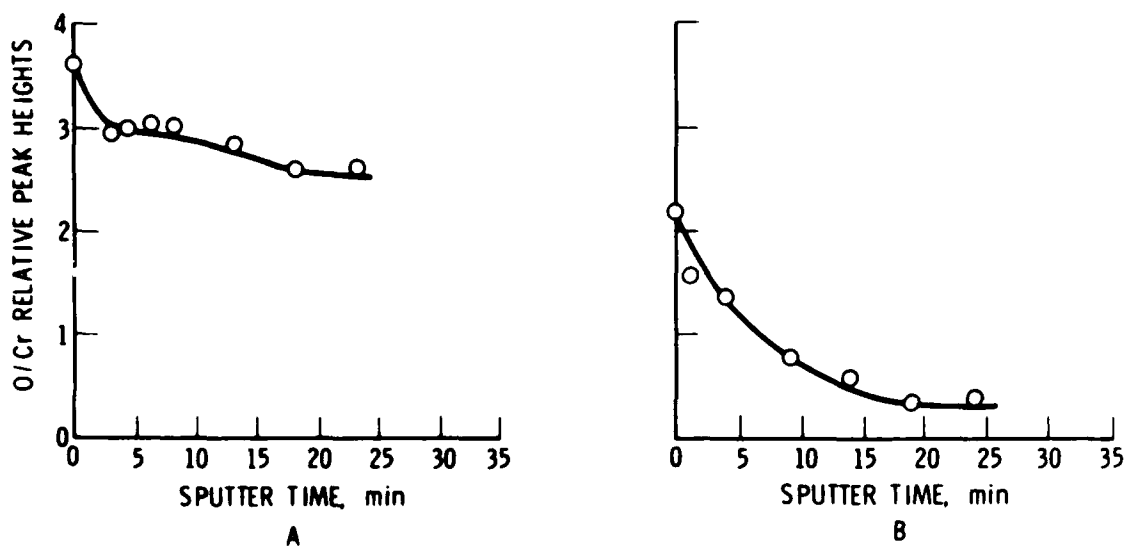


Fig. 37. Auger Surface Profiles of Black Cr on Cr on Mo, Showing Oxygen Depth Profile. (a) Laboratory control sample, showing oxygen content of oxide. (b) STS-8 flight sample, showing exposed Cr substrate.



Fig. 38. Photomicrograph of Mo/Cr/Black Cr Sample, Showing Debonding of Surface Layer and Exposed Cr Undercoating

to determine if the Mo was exposed. Another possible cause of debonding under the beam may be local heating, leading to thermal stresses that might also cause detachment of the scale when there is a reduced adherence to the surface. In summary, adherence changes are seen in the oxygen ram-exposed samples, but no major induced microstructural or compositional effects are found. Thus, the cause of the reduced adherence is not fully apparent.

Depth profiling of oxygen on the black Ir coating flown on STS-8 (Fig. 39) showed a decrease in oxygen by a factor of about two, going from the immediate surface into the bulk. SEM observation showed a "furrowed" surface (Fig. 40a) after atomic oxygen exposure, compared to the control sample (Fig. 40b), indicating some attack of the surface has occurred. In addition, regions of exposed substrate were observed.

No major microstructural damage was seen in the black Rh coating, as compared to the black Ir coating. However, at low magnification the coating exhibited a pattern of ring-like mottling (Fig. 41) whose origin is uncertain, suggestive of an etching effect. It has been noted that varied surface morphologies can arise as a result of sputtering of surfaces under various conditions; these morphologies include cones, rods, hillocks, and other structures.¹⁴

The samples of KAT glass showed no major microstructural changes caused by the exposure. A comparison of the STS-8 and lab control samples is shown in Fig. 42.

E. CONCLUSIONS

High-temperature coatings underwent some changes as a result of exposure to the atomic oxygen environment in the STS-8 experiment. Large changes occurred in the black metal samples. This may be supported by the fact that previous and ongoing studies have shown that the black Ir and Rh samples prepared by sputter deposition are unstable at elevated temperatures, undergoing microstructural changes that are associated with changes in reflectivity. The increase in reflectivity of the black Cr coating is probably due to the exposure of the metallic substrate, because atomic oxygen erodes the coating.

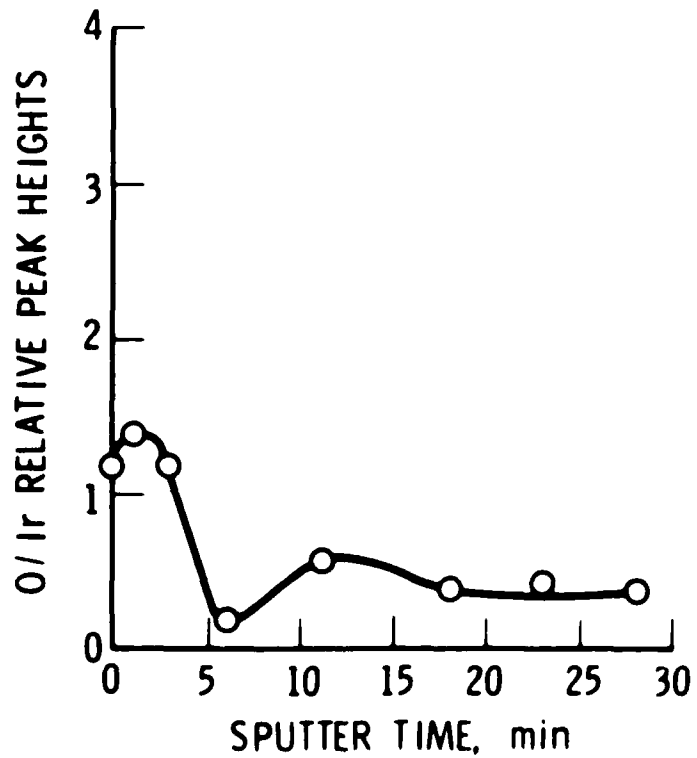


Fig. 39. Auger Depth Profile of Black Ir Coating, Showing Oxygen Depth Profile

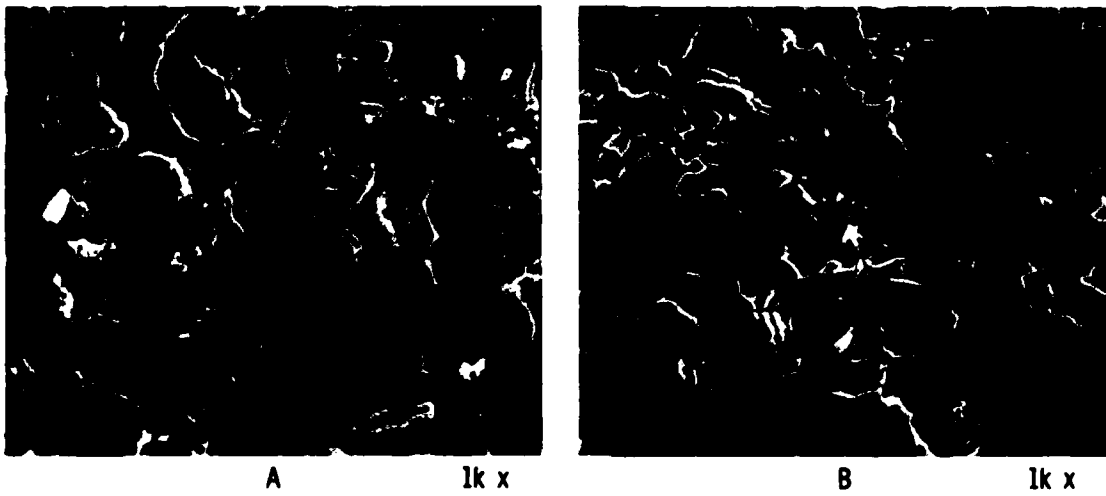
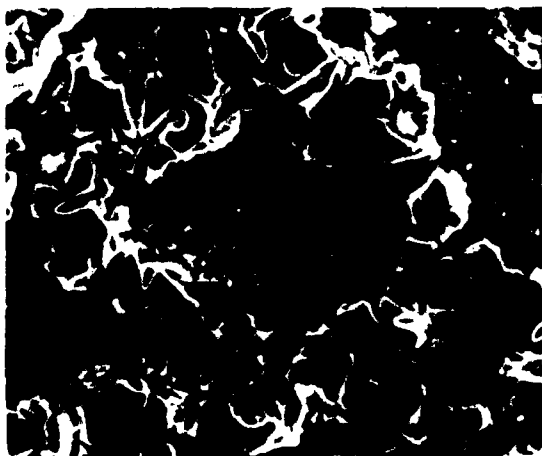


Fig. 40. Scanning Electron Micrographs of Black Ir on Mo Coating. (a) Laboratory control sample and (b) STS-8 flight sample, showing "furrowing" caused by exposure to atomic oxygen.



40 x

Fig. 41. Photomicrograph of Black Rh on Mo Coating of STS-8 Flight Sample, Showing Pattern of Ring-Like Mottling



A 300 x



B 300 x

Fig. 42. Photomicrographs of KAT Glass on Mo Coating. (a) Laboratory control sample. (b) STS-8 flight sample.

Further work will involve examining the diffuse reflectance of the materials in the 0.3 to 25 μm range (30000 to 400 cm^{-1}) to determine the solar absorptance (α_s) and thermal emissivity (ϵ).

REFERENCES

1. J. T. Visentine, L. J. Leger, J. F. Kuminecz, and I. K. Spiker, "STS-8 Atomic Oxygen Effects Experiment," paper presented at AIAA 23rd Aerospace Sciences Meeting, Reno, Nev. (January 1985).
2. G. S. Arnold, R. R. Herm, and D. R. Peplinski, "Atmospheric Effects in Low Earth Orbit and the DMSP ESA Offset Anomaly," SD-TR-82-81, The Aerospace Corporation (30 September 1982).
3. J. C. Bailar, H. J. Emeleus, Sir Ronald Nyholm, and A. F. Trotman-Dickenson, Comprehensive Inorganic Chemistry, Vol. 3 (Pergamon Press, 1973), p. 229.
4. L. J. van der Pauw, "A Method of Measuring Specific Resistivity and Hall Effect of Discs of Arbitrary Shape," Philips Res. Rep. 13, No. 1 (1958).
5. Westinghouse Electric Corporation, Defense and Electric Systems Center, Specification #9RA3974 (30 October 1979).
6. M. R. Comer, Westinghouse Electric Corporation, private communication.
7. R. J. Diefendorf and E. Tokarsky, "High-Performance Carbon Fibers," Polymer Engineering and Science 15 [3] (1975).
8. G. S. Arnold and D. R. Peplinski, "A Facility for Investigating Interactions of Energetic Atomic Oxygen with Solids," ATR-84(8540)-3, The Aerospace Corporation (16 September 1985).
9. P. N. Peters, R. C. Linton, and E. R. Miller, "Results of Apparent Atomic Oxygen Reactions on Ag, C, and Os Exposed during the Shuttle STS-4 Orbits," Geophys. Res. Lett. 10, 569-571 (1983).
10. G. D. Pettit, J. J. Cuomo, T. H. DiStefano, and J. M. Woodall, "Solar Absorbing Surfaces of Anodized Dendritic Tungsten," IBM J. Res. Dev. 22, 372-377 (1978).
11. G. Zajac and A. Ignatiev, "Percolation-Type Behavior in Black Chrome Selective Solar Films," Appl. Phys. Lett. 41, 435-437 (1982).
12. "Standard Methods for Measuring Adhesion by Tape Test," American National Standard ASTM D3359-78.
13. C. M. Lampert, "Metallurgical Analysis and High-Temperature Degradation of the Black-Chrome Solar-Selective Absorber," Thin Solid Films 72, 73-81 (1980).
14. R. S. Berg and G. J. Kominiak, "Surface Texturing by Sputter Etching," J. Vac. Sci. Tech. 13, 403-405 (1976).

LABORATORY OPERATIONS

The Aerospace Corporation functions as an "architect-engineer" for national security projects, specializing in advanced military space systems. Providing research support, the corporation's Laboratory Operations conducts experimental and theoretical investigations that focus on the application of scientific and technical advances to such systems. Vital to the success of these investigations is the technical staff's wide-ranging expertise and its ability to stay current with new developments. This expertise is enhanced by a research program aimed at dealing with the many problems associated with rapidly evolving space systems. Contributing their capabilities to the research effort are these individual laboratories:

Aerophysics Laboratory: Launch vehicle and reentry fluid mechanics, heat transfer and flight dynamics; chemical and electric propulsion, propellant chemistry, chemical dynamics, environmental chemistry, trace detection; spacecraft structural mechanics, contamination, thermal and structural control; high temperature thermomechanics, gas kinetics and radiation; cw and pulsed chemical and excimer laser development including chemical kinetics, spectroscopy, optical resonators, beam control, atmospheric propagation, laser effects and countermeasures.

Chemistry and Physics Laboratory: Atmospheric chemical reactions, atmospheric optics, light scattering, state-specific chemical reactions and radiative signatures of missile plumes, sensor out-of-field-of-view rejection, applied laser spectroscopy, laser chemistry, laser optoelectronics, solar cell physics, battery electrochemistry, space vacuum and radiation effects on materials, lubrication and surface phenomena, thermionic emission, photo-sensitive materials and detectors, atomic frequency standards, and environmental chemistry.

Computer Science Laboratory: Program verification, program translation, performance-sensitive system design, distributed architectures for spaceborne computers, fault-tolerant computer systems, artificial intelligence, microelectronics applications, communication protocols, and computer security.

Electronics Research Laboratory: Microelectronics, solid-state device physics, compound semiconductors, radiation hardening; electro-optics, quantum electronics, solid-state lasers, optical propagation and communications; microwave semiconductor devices, microwave/millimeter wave measurements, diagnostics and radiometry, microwave/millimeter wave thermionic devices; atomic time and frequency standards; antennas, rf systems, electromagnetic propagation phenomena, space communication systems.

Materials Sciences Laboratory: Development of new materials: metals, alloys, ceramics, polymers and their composites, and new forms of carbon; non-destructive evaluation, component failure analysis and reliability; fracture mechanics and stress corrosion; analysis and evaluation of materials at cryogenic and elevated temperatures as well as in space and enemy-induced environments.

Space Sciences Laboratory: Magnetospheric, auroral and cosmic ray physics, wave-particle interactions, magnetospheric plasma waves; atmospheric and ionospheric physics, density and composition of the upper atmosphere, remote sensing using atmospheric radiation; solar physics, infrared astronomy, infrared signature analysis; effects of solar activity, magnetic storms and nuclear explosions on the earth's atmosphere, ionosphere and magnetosphere; effects of electromagnetic and particulate radiations on space systems; space instrumentation.